EFFECT OF PRESSURE-DEPENDENT PERMEABILITY ON TIGHT GAS WELLS

A Thesis

by

MARIELA FRANQUET BARBARA

Submitted to the Office of Graduate Studies of
Texas A&M University
in partial fulfillment of the requirements for the degree of

MASTER OF SCIENCE

May 2004

Major Subject: Petroleum Engineering

EFFECT OF PRESSURE-DEPENDENT PERMEABILITY ON TIGHT GAS WELLS

A Thesis

by

MARIELA FRANQUET BARBARA

Submitted to the Office of Graduate Studies of
Texas A&M University
in partial fulfillment of the requirements for the degree of

MASTER OF SCIENCE

Approved as to style and content by:

Robert A. Wattenbarger (Co-Chair of Committee)	J. Bryan Maggard (Co-Chair of Committee)
Wayne M. Ahr (Member)	Stephen A. Holditch (Head of Department)

May 2004

Major Subject: Petroleum Engineering

ABSTRACT

Effect of Pressure-Dependent Permeability on Tight Gas Wells. (May 2004)
Mariela Franquet Barbara, B.S., Universidad Simon Bolivar
Co-Chairs of Advisory Committee: Dr. Robert A. Wattenbarger
Dr. J. Bryan Maggard

Tight gas reservoirs are those reservoirs where the matrix has a low permeability range ($k < 0.1$ md). The literature documents laboratory experiments under restressed conditions that show stress dependent rock properties are more significant in tighter rocks. For gas reservoirs, real gas properties are also sensitive to variations of pressure, and the correct description of gas flow must include pressure-dependent gas properties. Under these circumstances the resulting equation for real gas flow is a second order, non-linear, partial differential equation. Non-linearities include pressure-dependence of gas viscosity, gas compressibility, reservoir permeability and reservoir porosity.

This paper investigates dynamic permeability change as a function of net overburden stress in tight gas reservoirs. The gas reservoir simulator used for this work included pressure–dependent reservoir permeability. Radial flow cases are analyzed using this simulator.

During this study we found that from analysis of production data alone, it is impossible to determine the correct permeability value for tight gas reservoirs with pressure-dependent permeability. For the cases studied, the transient performance was similar for both constant permeability and pressure-dependent permeability. This similarity causes constant permeability and pressure-dependent permeability to be indistinguishable, based on analysis of transient performance data.

It was found that the productivity index decreases when pressure-dependent permeability is more significant. Finally, this study verified that the method of Ibrahim e*t al*.[28] under estimates original gas in place (*OGIP*) for tight gas reservoirs with pressure-dependent permeability.

DEDICATION

I wish to dedicate my thesis:

First to God, Jesus and Mary who have been guiding my life,
I thank you Father for so many blessings;

To my parents, Francisco and Martha for all their support, encouragement, sacrifice,
and especially for their unconditional love, I love you both;

To my brothers, David and Javier for their help, caring
and the great moments we spent together, I love you too.

and

To my true love David, who has been a special blessing.

ACKNOWLEDGMENTS

I wish to express my sincere gratitude and appreciation to:

Dr. Robert A. Wattenbarger, chair of my advisory committee, for his continued help and support throughout my research. It was great to work with him.

Dr. J. Bryan Maggard, co-chair of my advisory committee, for his enthusiastic and active participation and guidance during my investigation. Also, for giving me the opportunity to work with him as his T.A. for ENGR-211. It was a great experience.

Dr. Wayne Ahr, for his encouragement to my research, his motivation to continue studying and his always-good mood.

Dr. Blasingame, for his support, his wise words and unconditional advice. Thank you so much. You were right when you said, 'you can make it'.

El Paso Company, for giving me the opportunity to improve my knowledge in Petroleum Engineering.

Finally, I want to express my gratitude and appreciation to all my colleagues at Texas A&M University: Mazher Ibrahim, Adriana Ovalle, Claudia Soto, Deji Adeyeye, Christian Huapaya, and Romi Triaji Branajaya.

TABLE OF CONTENTS

Page

CHAPTER Page

LIST OF FIGURES

FIGURE Page

FIGURE Page

FIGURE Page

LIST OF TABLES

TABLE Page

CHAPTER I

INTRODUCTION

1.1 Tight Gas Reservoirs

Unconventional reservoirs are those reservoirs that cannot be produced at economic flow rates or cannot produce enough volume of oil and gas without stimulation treatments or special recovery processes and technologies. The future energy resources of the United States, particularly gas, will be found in these kinds of reservoirs.

Tight gas is a type of unconventional reservoir that refers to natural gas production from reservoirs with low permeability.These reservoirs have been studied by many authors[1-30].

Natural gas is needed to meet increased world energy demand in the near future. And since it is expensive to drill wells, petroleum industry has been working hard to find ways to produce tight gas economically and efficiently from fewer wells.

Tight Gas Reservoirs present an average permeability of less than 0.1 md. A new definition for tight gas reservoirs defined by the German petroleum industry, includes reservoirs with average effective gas permeability less than 0.6 md. Wells completed in tight reservoir rocks have to be stimulated in order to achieve an economically adequate production rate. Other modern technologies for the production of tight gas reservoirs include horizontal and multilateral wells, as well as underbalanced drilling.

This thesis follows the style of the *SPE Reservoir Evaluation and Engineering Journal.*

Tight-gas wells are expected to have the following two unique flow characteristics:

1) Long transient flow period (time) due to the 'tight' permeability, and
2) Approximately linear 1-D 'flow geometry' due to the combined effects of 'tight' permeability and the practical necessity of hydraulic fracturing.

1.2 Gas Flow

For gas flow, real gas properties are a function of pressure, and the correct description of gas flow cannot neglect this fact. Under these circumstances the resulting equation for the real gas flow through porous media is a second, nonlinear, partial differential equation. This equation was reduced by a change of variables similar to the real gas pseudo-pressure of Al-Hussainy *et al.*[14] The power of this transformation lies in the fact that it linearizes the flow side of the real gas diffusivity equation.

1.3 Objectives

The main objective of this project is to determinate how dynamic permeability change as a function of stress in tight gas wells affects radial transient performance. And the specific objective is to document the implications of stress-sensitive permeability for gas production, based on reservoir simulation. These simulations will present evidence of the difficulty in distinguishing between constant reservoir permeability or pressure-dependent reservoir permeability case from field data.

The results of this work will allow us to have a better idea of the effects that pressure-dependent permeability have on tight gas reservoir performance.

1.4 Problem Description

Permeability is usually considered to be a constant value. However, permeability is sensitive to pressure changes, as shown in many laboratory experiments.

Simulation cases are presented in this work where permeability is considered to be a function of pressure. In the semi-log plots used to analyze transient performance, straight lines were observed, which made it difficult or impossible to distinguish between constant permeability and pressure-dependent permeability cases.

1.5 Motivation: Reservoirs of the Future

The motivation of this study is that gas reservoirs, specifically, tight gas reservoirs will be the future engineer's target to satisfy world energy demand. This gas will be found in what we consider today to be unconventional reservoirs, especially tight gas reservoirs in shales, siltstones, fine-grained sands, and carbonates. These are usually not considered to be undiscovered resources, since their occurrences are fairly well-known. However, we do not have adequate data to evaluate the contribution such reservoirs will make to the world energy supply in the future.

This is one of the motivations of this project: to better understand the behavior of this kind of reservoir and to improve the technology in preparation for future energy demand.

CHAPTER II

LITERATURE REVIEW

2.1 Introduction-Theory

As early as 1928, it was recognized that porous media are not always rigid and non-deformable. This problem is usually handled by means of properly chosen 'average' properties. This method only reduces the errors involved and generally does not eliminate these errors. Classical treatments solve the linear diffusivity equation, which assumes that diffusivity is constant (independent of pressure). When both pressure changes and property changes are small, the constant-property assumption is justified. But if rock and fluid property changes are significant over the pressure range of interest, these changes cannot be neglected and a variable-property solution is needed.

Samaniego *et al.*[5] investigated the effects of pressure-dependent fluid properties and stress-sensitive rock properties on pressure transient analysis. They presented results of an investigation of the application of the *m(p)* method to drawdown, buildup, and injection testing. Results were obtained for five different sets of rock and fluid properties. They concluded that the *m(p)* function is an excellent 'linearizing' tool for constant production rate pressure transient tests for all practical flow rates.

Vairogs *et al.*[1] measured flow rates in tight gas reservoirs and observed that measured flow rates are sometimes much lower than predicted by transient gas flow equations based on Darcy's law. Several explanations for this discrepancy have been offered:

1. Errors may be caused by invalid assumptions such as reservoir homogeneity, open-hole completions, and single-phase flow.
2. Non-Darcy effects due to high gas velocity near the wellbore may restrict flow.

Vairogs *et al.*[1] conducted their study in order to: 1) To confirm the conclusions of previous work[7,8,15-17] and to demonstrate experimentally that permeability reduction is proportionately greater in low-permeability than in high-permeability cores. 2) To incorporate the stress effects into a mathematical model for reservoir gas flow. 3) To use this model to check the extent of production decrease that might be expected due to pressure-dependent permeability.

When gas is produced from reservoirs, the pore pressure decreases and the net confining stress on the reservoir rock increases. The compaction due to increasing net confining stress causes reduction in effective pore diameters, resulting in a reduced permeability.

In 1983 Ostensen analyzed the effect of microcrack permeability in several tight gas sandstones and concluded that the stress dependence of permeability in these tight-gas-sand cores is controlled by flow through microcracks.[20] Also that permeability can be correlated by a Jones-and-Owens-type correlation[21] using the square root, varying linearly with the log of confining stress.[20]

The net confining stress on the rock increases as the gas pressure in the reservoir decreases, so the reservoir flow capacity decreases during gas production. This can cause anomalous behavior during well tests. The well-test and gas-production behavior of a stress-sensitive gas reservoir were first studied by Vairogs *et at.*[1], whom developed a reservoir simulator that also calculated the approximate effect of rock stresses in the reservoir resulting from changes in gas pressure. They showed that reduction of production rate by as much as 50% were possible. This work assumes that the stress dependence of cores is characteristic of the reservoir and extends the work of Vairogs *et al.*[1] and Vairogs and Rhodes[2] by deriving general results for the effect of stress dependence on well test analysis and gas production.

The increase in emphasis in the Petroleum industry on transforming partial differential equations is probably due to the real gas pseudo-pressure concept introduced by Al-Hussainy *et al.*[14] in 1966. Their definition of real gas pseudo-pressure, $m(p)$, is:

$$m(p) = 2\int_{p_o}^{p} \frac{p}{\mu(p)z(p)}\,dp \quad \text{.....(2.1)}$$

The basic objective of equation 2.1 was to transform non-linear differential equations to a form similar to diffusion-type equations. The literature indicates that pressure-dependent permeability can be included in the definition of pseudo-pressure. The partial differential equation for a pressure-dependent reservoir has been discussed by Matthews and Russell[29].

Raghavan *et al.*[4] considered transient radial flow of variable-property liquids in a reservoir where the compressibility, porosity and permeability are arbitrary functions of pressure when the outer boundary is impermeable (closed). Their main objective was to obtain a solution to this problem that could be applied for engineering purposes, provided the pseudo-pressure function, using hand calculations.

Fatt[6] reported pore volume compressibilities measured in the laboratory on core samples for a typical reservoir sandstones at reservoir pressures. These compressibilities are different for each reservoir sample and cannot be correlated to porosity. The compressibilities are also a function of pressure.

Gray *et al.*[7] showed that permeability anisotropy of several sandstones is a function of overburden pressure. Studies on Berea and Bandera sandstone showed that permeability of these materials decreases upon application of simulated overburden pressure.

Sensitivity of permeability to pore pressure is often a key factor in formation evaluation of tight gas sands[1]. Gas permeability reductions of more than an order of magnitude have been observed in dry cores when net overburden pressure is increased to typical formation values. Although this sensitivity to pressure has been related to the presence of clays and shales, the current consensus is that the pressure behavior of crack-shaped pores (pores characterized by two large dimensions and one small) is largely responsible.

Brower *et al.*[9] examined the effect of pressure on pore structure and consequent changes in gas permeability for a variety of natural and synthetic porous media.

Ostensen[3] assumed that information from core analysis is applicable to reservoir behavior. Because microcracks are the primary path for flow through tight-gas-sand cores, average stress-dependent permeabilities were found as an average over all crack orientations in a non-uniform stress field, with a horizontal stress only 0.6 times the vertical stress. Initial in-situ permeabilities are found to be two to five times the values obtained from uniformly restressed cores. Stress dependence reduces initial gas production by at most 30%, with the reduction increasing during reservoir depletion.

Ostensen[20] developed a model of stress-dependent permeability on the basis of flow through cracks. The relative reduction of permeability is frequently as much as a factor of ten. This corresponds with the observation that flow rates in tight-gas reservoirs are frequently much lower than predictions based on routine core-analysis data.

Pinzon *et at.*[10] presented an analysis of a field isochronal test. The effect of stress-sensitive permeability on well test response was analyzed through numerical simulations. Guidelines useful in identifying stress-sensitivity permeability from well testing were proposed. The following objectives were pursued in this study: 1) investigate how to recognize stress sensitive-permeability from pressure transient testing, and 2) analyze field well test data in terms of diagnosis of stress-sensitive permeability.

Kikani and Pedrosa[12] presented the use of a regular perturbation technique to solve the nonlinear equation to the third order of accuracy. It was demonstrated that the third-order term is of the same order of magnitude as the second-order term and thus needs to be included in the solution, although the net result on the dimensionless pressure solution is quite small. Also they investigated the first-order effects of wellbore-storage,

skin, and boundary effects. A field example was analyzed to determine the permeability modulus (γ) and reservoir properties.

Another approach to the nonlinear problem with stress-dependent permeability was defining the permeability modulus[30] similar to the definition of compressibility:

$$\gamma = \frac{1}{k}\frac{\partial k}{\partial p} \quad \text{.....(2.2)}$$

Equation 2.2 gives a particular function of permeability that is an exponential function of pressure.

Production from a stress-sensitive reservoir will create a zone of increasing effective stress and reduced permeability in the low-pressure region near the wellbore. This is expected to a positive skin factor. The skin factor is the combination of the mechanical skin factor, and skin factor due to a stress-sensitive permeability. Permeability due to stress change can be the dominating factor that influences well response in stress-sensitive reservoirs if the rock compressibility is not significant.

2.2 Laboratory Experiments of Stress Effect on Permeability

Several authors[1] have studied the reduction of permeability due to rock stress. In the Vairogs *et al.*[2] study, confining pressures were applied hydrostatically and with different pressure applied to the sides of the core than to the ends. The effect of stress on the only core that presented less than 0.1 md permeability was much greater than the effect on the others. The explanation given for that was that very tight cores have smaller pore radii. Increasing the compressive stress applied to pores of small radius could decrease their flow capacity proportionately more than that of large pores. These laboratory experiments were demonstrated experimentally that permeability reduction is proportionately greater in low-permeability than in high-permeability cores.

Permeability measurements were made at several levels of confining pressure for each core by flowing nitrogen through it[1]. The nitrogen was introduced at a constant pressure of 150 psig. Fig. 2.1 and 2.2 show some general observations made during the course of the study. Each plot had k/k_i, the ratio of permeability at a given confining pressure to the permeability at a confining pressure of 500 psig, as a function of confining pressure. The 500 psig initial confining pressure was the initial condition for each series of permeability measurements. (see Vairogs *et al.*[1])

Fig. 2.1 illustrates the greater degree of permeability reduction with low-permeability cores than with high-permeability cores. Core A is Chanute sandstone, Core B is San Andres carbonate, Core C and D are Springer sandstone, and Core E is Frio sandstone. Previous work by Davies and Davies reveals that diagenesis is a fundamental control on the pore geometry and stress sensitivity of consolidated sandstone reservoirs. Diagenesis is known to vary with changes in 1) depositional environment, 2) stratigraphic position, 3) the location of structural elements such as faults, joints, flexures and 4) relative to the location of the structural crest. Thus an understanding of the lateral and vertical diagenetic trends in a field is of significance to understanding the distribution of stress dependent permeability within any reservoir. A detailed knowledge of diagenesis becomes critically important in large, stratigraphically or structurally complex

consolidated reservoirs where several different episodes of diagenesis may characterize a single stratigraphic layer.

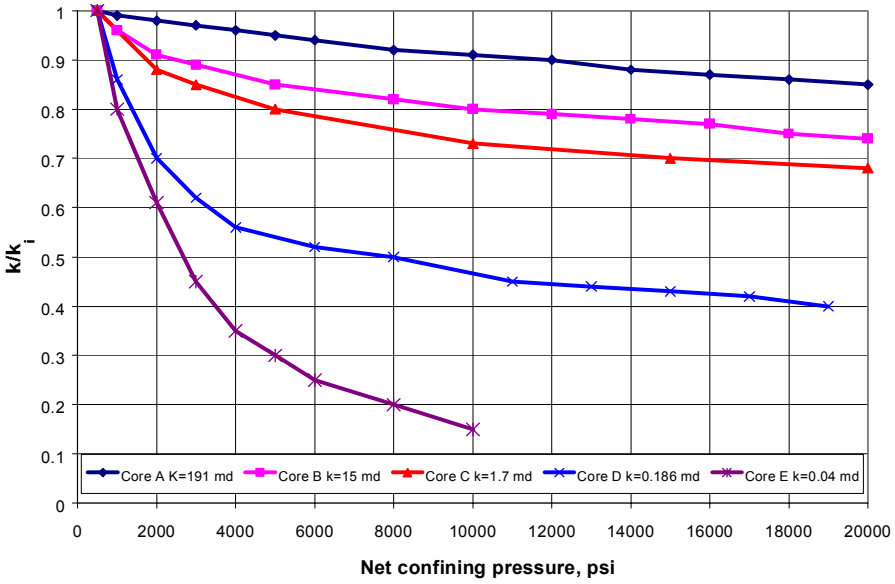

Fig. 2.1-Permeability ratio versus net confining pressure *(Vairogs).*

The presence of shale streaks and hairline fractures appeared to drastically increase the permeability reduction due to stress. This phenomenon can be seen in Fig. 2.2 where Core F is Springer sandstone laminated with shale streaks and exhibiting hairline fractures.

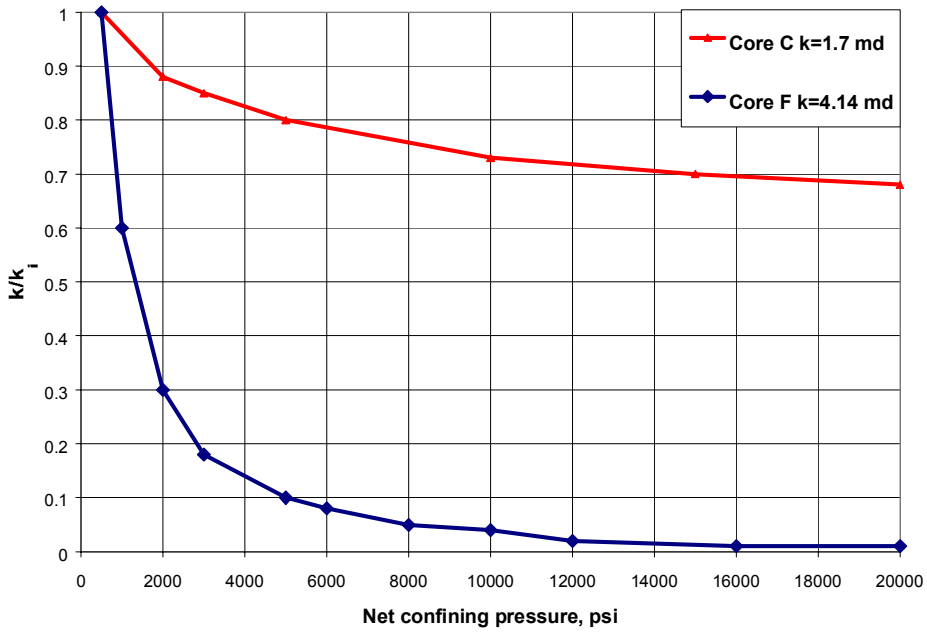

Fig. 2.2-Permeability ratio versus net confining pressure.

Fig. 2.3 shows the hysteresis effect for a Morrow sandstone core (Core J). This figure shows permeability at specified stress levels (solid line) and the permeability after the confining pressure was quickly reduced to 500 psig (dotted lines).

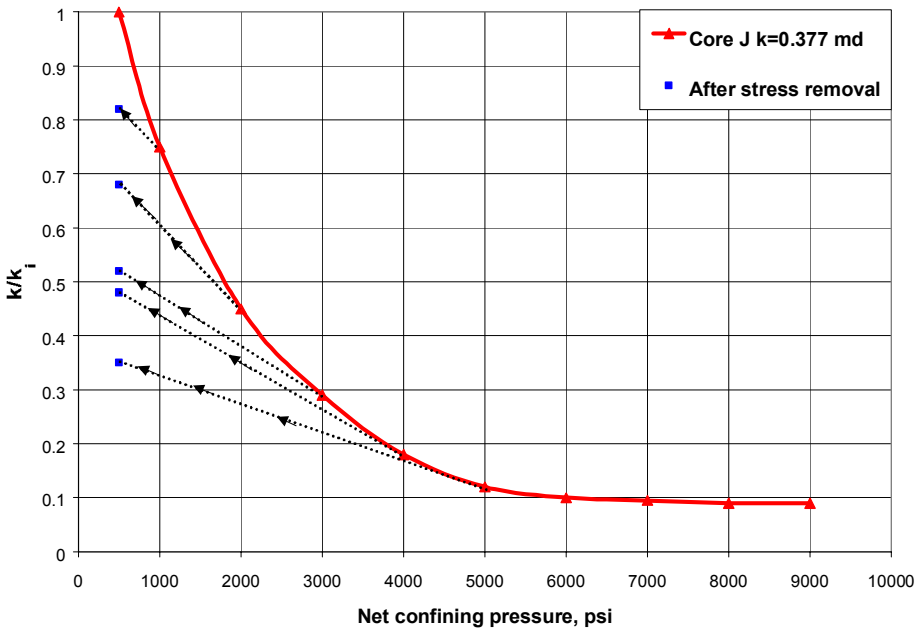

Fig. 2.3-Hysteresis effect after stress removal.

From these laboratory experiments, it can be concluded that 1) When the stress effect is significant most of the loss of permeability occurs by the time the net confining stress level reaches about 4,000 psi. 2) The permeability of a rock may depend on confining pressure in a complex manner.

In the experimental measurements, the confining pressure was applied uniformly in all directions. Since the pore pressure during the flow test was very low, the confining pressure is the rock stress.

2.3 Reservoir Compaction and Permeability

The evolution of the stress state in a depleting reservoir has a significant influence on the changes in physical properties within the reservoir. Reservoir compaction and surface subsidence are caused by volumetric changes in the reservoir pore space, brought about by reservoir pressure reduction during production.

To assess the magnitude of these changes, the rock's volumetric compressibilities (grain, bulk and pore volume compressibilities) are determined. These values are also essential for estimation of gas in place, reservoir maintenance and production drive assessments. Poor appreciation of the mechanics of rock compressibility under various states of stress (i.e., hydrostatic compression or uniaxial strain compression) may result in predictions with substantial errors. Fig. 2.4 shows the effect of overburden pressure. Stage 'a' represents the rock without stress effects, Stage 'b', 'c' and 'd' represent the same rock under increasing stress.

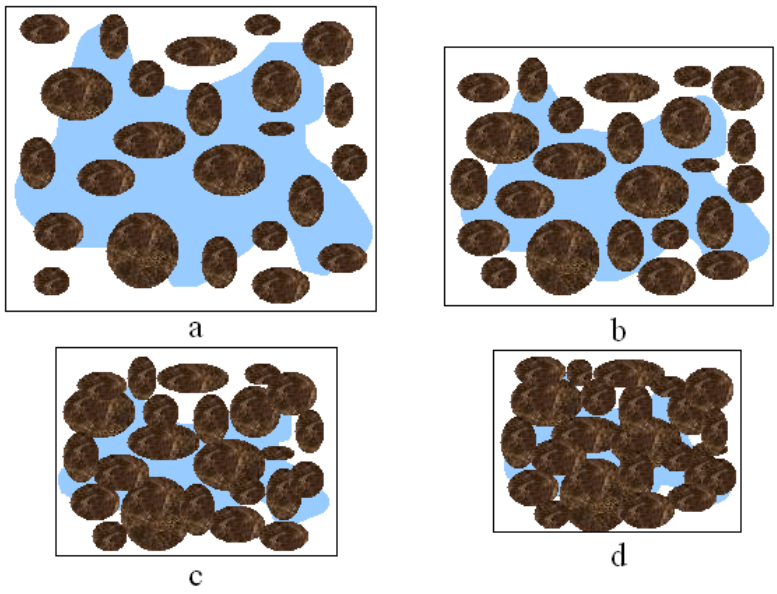

Fig. 2.4-Compaction effect with overburden pressure.

2.4 Parameters Inducing Reservoir Compaction

The parameters that influence induced reservoir compaction and deformation are:

1) Overburden pressure, which is acting on the reservoir rock grain resisting the in-situ stress, up to failure pressure or grain crush.
2) Reservoir rock characteristics that play an important role in rock mechanics.
3) Wetting fluid covering the cement integain bond, which has influence on mechanical rock properties.
4) Rocks having different porosities behave differently under similar stress conditions, since there is a different contact area between grains per unit bulk rock volume. Therefore rocks having lower porosity are typically more resistant to compaction than high porosity rocks.
5) Pore-pressure acts in the direction opposite overburden stress and therefore the effective stress consists of the difference between the two.
6) Horizontal or diagonal reservoir stresses, originally in equilibrium, which becomes active as reservoir pressure drops.
7) Structural dip angle of the formation may have a strong influence on the initial deformation rate during reservoir's pressure depletion.
8) Presence of active movement like plate tectonic activity could be an element of the stresses during reservoir history.

To up-scale the laboratory results and complicated well measurements to actual field dimensions, while including all of the above-mentioned parameters, is extremely complicated if not impossible at the present time.

CHAPTER III

FUNDAMENTALS

3.1 Permeability Modulus

To study fluid flow through stress dependent porous media, a new parameter, the permeability modulus or 'γ', is defined by Nur *et al.*[30] and studied by Kikani *et al.*[12] as follows:

$$\gamma = \frac{1}{k}\frac{\partial k}{\partial p} \qquad \text{.....(3.1)}$$

This parameter plays a very important role in systems where changes in effective stress affect permeability. Basically, it measures the dependence of hydraulic permeability on pore pressure. For practical purposes, the permeability modulus is assumed constant. Thus, permeability varies exponentially with pore pressure.

$$k = k_i e^{-\gamma(p_i - p)} \qquad \text{.....(3.2)}$$

In view of the similar appearance of permeability and density in the diffusion equation, it may be advantageous to assume an exponential relationship between permeability and pressure. This choice has some experimental support and mathematical convenience as suggested by Kikani and Pedrosa[12]. These authors were able to match an exponential rock model to real pressure data.

Experimental data from Vairogs and Rhoades[2] showed that permeability reduction ratio as an exponential function of pressure fits reasonably well. Fig. 3.1 shows this behavior.

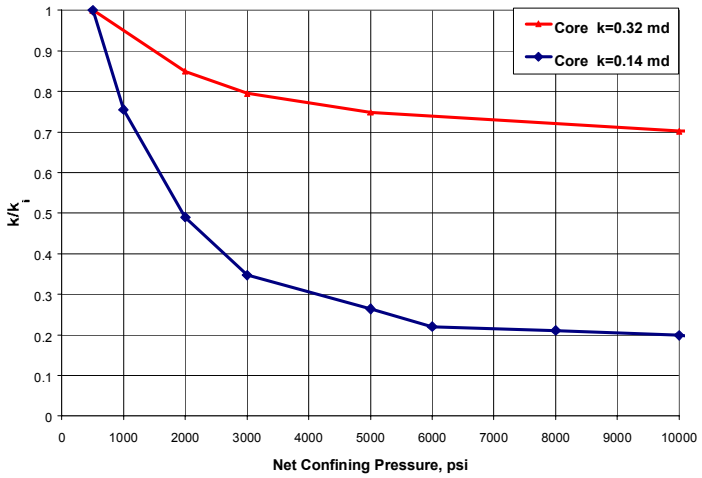

Fig. 3.1-Permeability reduction as a fraction of permeability at confining stress of 500 psi.

The permeability ratio is denoted as k/k_i in Fig. 3.1, where k is the calculated permeability and k_i is the initial permeability. The most relevant observation in Vairogs and Rhoades[2] work was that cores with lower permeability are more sensitive to pressure changes as it is shown in Fig. 3.1.

3.2 Gas Simulator

GASSIM is a single-phase simulator presented by Lee and Wattenbarger[33], and Wattenbarger *et al.*[31] It is used in this work for simulating real gas flow for radial cases. It is a two-dimensional reservoir simulator that can work with x-y or r-z geometries. Originally this program was written in FORTRAN.

This simulator has been modified and it is under development. For this work, a VBA (Visual Basic for Applications) version of GASSIM was modified to include permeability module. This modified version of GasSim was used to run all the cases presented in the next chapter.

CHAPTER IV

SIMULATION CASES AND RESULTS

In this chapter simulation results including pressure-dependent permeability for constant bottom-hole pressure and constant rate radial flow are investigated. First a radial infinite acting reservoir case was run with constant permeability. This case was run for both, constant bottom-hole pressure and constant gas production rate. Another case consists in a radial closed (finite acting) reservoir. The effect of pressure-dependent permeability on original gas in place calculations was investigated for both constant bottom-hole pressure and constant gas production rate.

4.1 Simulation Case 1: Infinite Acting – Constant p_{wf}

Case 1 is a radial flow case where the well in located in the center of the reservoir. It is infinite acting and the bottom-hole pressure is kept constant at 4,000 psi. Table 4.1 summarizes other characteristics of the reservoir. See Appendix A for complete GASSIM data.

Table 4.1- Main Characteristics of the Reservoir - Simulation Case 1.

Reservoir characteristic	Values
Initial porosity	15%
Initial reservoir pressure	8,800 psi
Initial permeability	0.0025 md
Initial total compressibility	3.49E-5 1/psi
Reservoir temperature	750 °R
Bottom-hole pressure	4,000 psi
Reservoir thickness	362 ft

Fig. 4.1 shows the plot of m_D versus t_{DA} for constant permeability ($\gamma = 0$). The plot has a semi-log straight-line indicating that the reservoir is infinite acting (transient period). Here t_{DA} and m_D are defined as:

$$t_{DA} = \frac{0.00633kt}{\phi\mu c_t A} \quad \text{.....(4.1)}$$

$$m_D = 1/q_D = \frac{kh\left[m(p_i) - m(p_{wf})\right]}{1422qT} \quad \text{.....(4.2)}$$

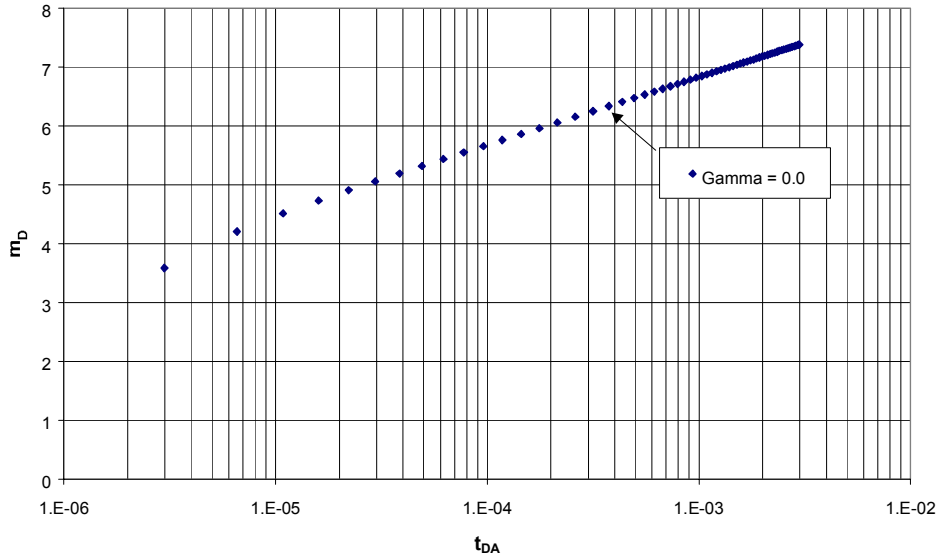

Fig. 4.1- Constant permeability case of m_D as a function of t_{DA} for an infinite acting reservoir producing at constant p_{wf}.

Fig. 4.2 shows the same results for constant permeability ($\gamma = 0$) and constant p_{wf}. For this case a straight line is obtained and the correct permeability value was calculated from the slope. See Appendix B for calculation details.

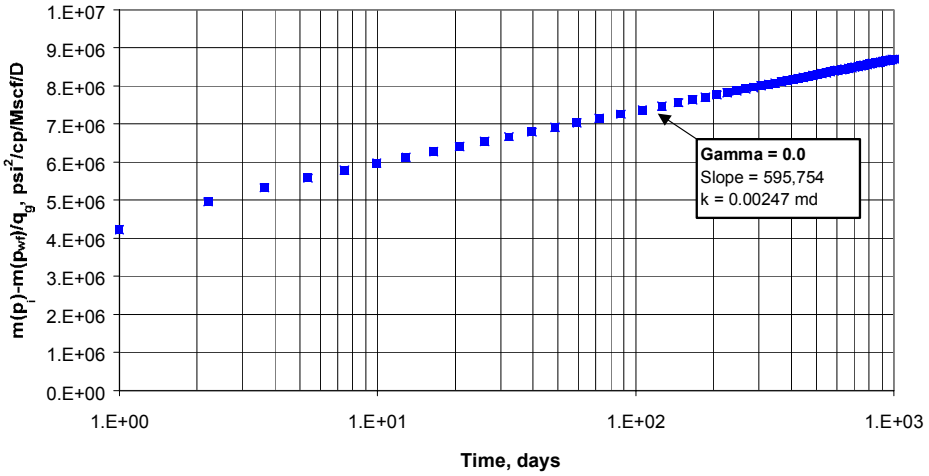

Fig. 4.2- Constant permeability case of $m(p_i)-m(p_{wf})/q_g$ as a function of time for an infinite acting reservoir producing at constant p_{wf}.

Next, pressure-dependent permeability was simulated. Permeability was calculated using equation 3.2. Fig. 4.3 shows semi-log straight lines for all cases. For each permeability modulus values the reservoir behaves as an infinite acting reservoir.

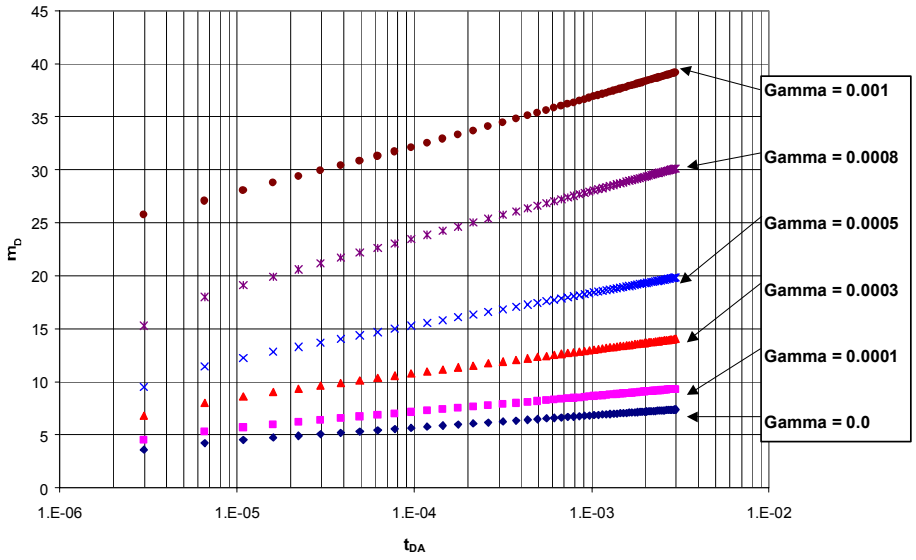

Fig. 4.3- Effect of pressure-dependent permeability for an infinite acting reservoir producing at constant p_{wf}.

Fig. 4.4 shows the different results for six values of permeability modulus. While permeability modulus values change to $1x10^{-4}$, $3x10^{-4}$, $5x10^{-4}$, $8x10^{-4}$ and $1x10^{-3}$, different straight lines were obtained with different slopes.

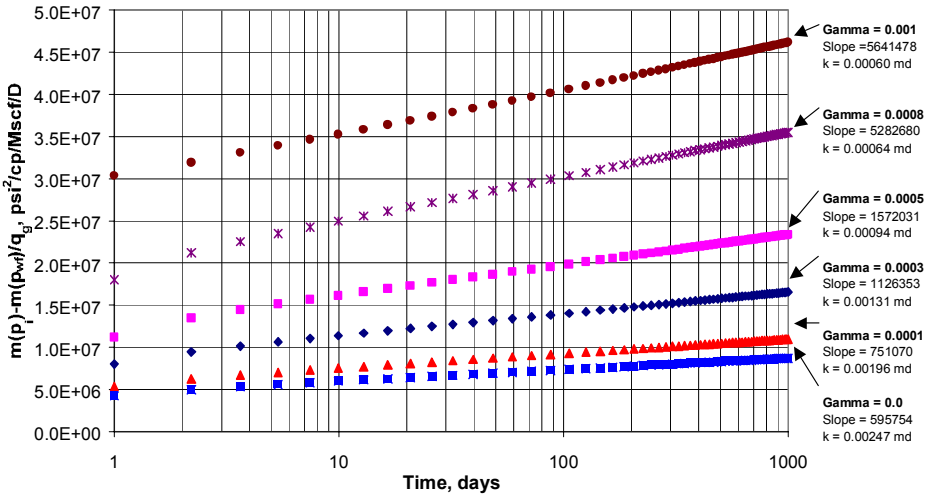

Fig. 4.4- Comparison of constant permeability with pressure-dependent permeability. Plot $m(p_i)-m(p_{wf})/q_g$ as a function of time for an infinite acting reservoir producing at constant p_{wf}.

This means that for each permeability modulus, we can calculate different permeabilities. For each permeability modulus, a different slope is obtained and a different permeability value is calculated. Fig. 4.5 shows calculated permeability variation as a function of permeability modulus for Case 1. Permeability calculation details are provided in Appendix B.

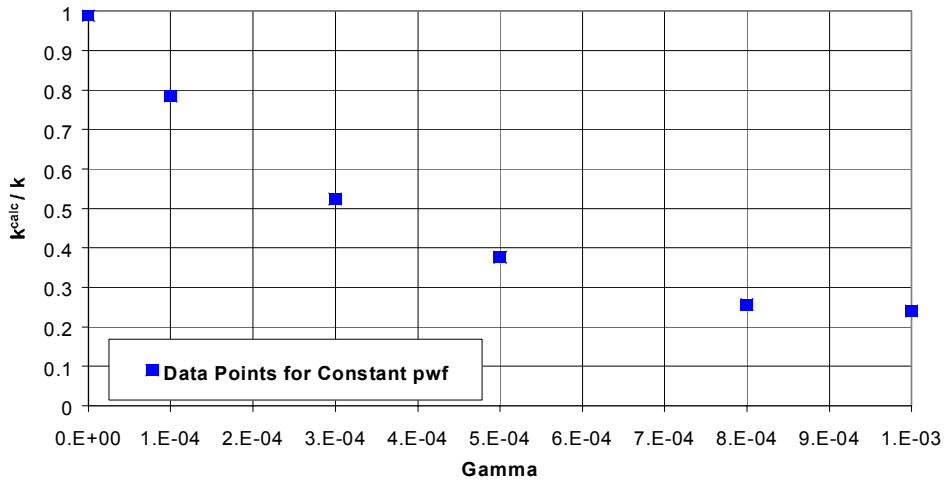

Fig. 4.5- Permeability ratio calculated on transient period versus permeability modulus for Simulation Case 1 and constant p_{wf}.

Fig. 4.6 shows the dimensionless skin values due to permeability reduction. Each skin value was calculated from the intercept (t = 1day) of the semi-log straight lines in Fig. 4.4. This result confirms that for higher permeability modulus values, more damage is observed.

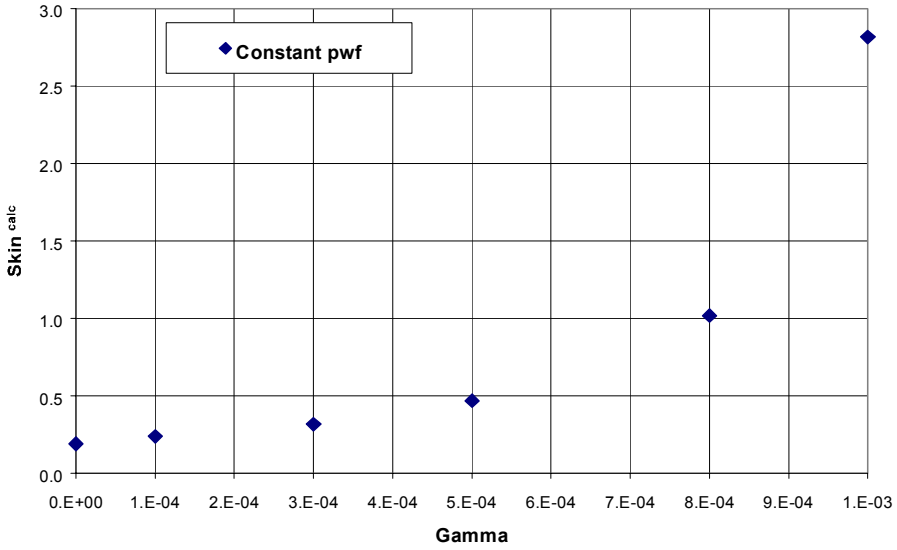

Fig. 4.6- Dimensionless skin versus permeability modulus for Simulation Case 1 and Constant p_{wf}.

4.2 Simulation Case 2: Infinite Acting – Constant q_g

Case 2 is a radial flow case with the well in located in the center of the reservoir. It is infinite acting and the gas rate is kept constant at 10,000 Mscf/D. Table 4.2 summarizes other characteristics of the reservoir. See Appendix A for the GASSIM data file.

Table 4.2- Main Characteristics of the Reservoir - Simulation Case 2.

Reservoir characteristic	Values
Initial porosity	15%
Initial reservoir pressure	8,800 psi
Initial permeability	0.0025 md
Initial total compressibility	3.49E-5 1/psi
Reservoir temperature	750 °R
Gas production rate	10,000 Mscf/D
Reservoir thickness	362 ft

Fig. 4.7 shows that for $\gamma = 0$ (constant permeability) a semi-log straight-line is observed; this confirmed that the reservoir is infinite acting (transient).

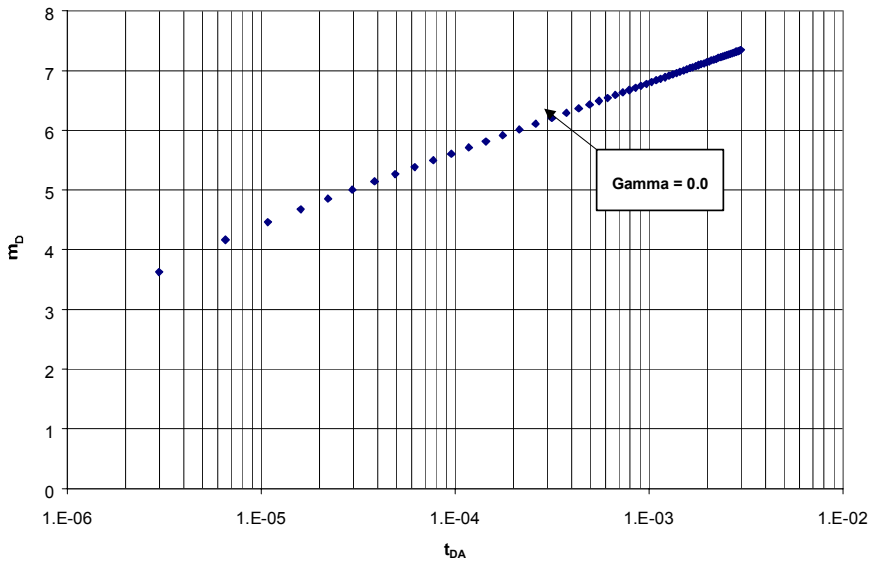

Fig. 4.7- Constant permeability case of m_D as a function of t_{DA} for an infinite acting reservoir producing at constant q_g.

Fig. 4.8 shows the same results for $\gamma = 0$ with constant q_g. For this case a straight line is obtained and the correct permeability value was calculated from the slope (see Appendix B for details).

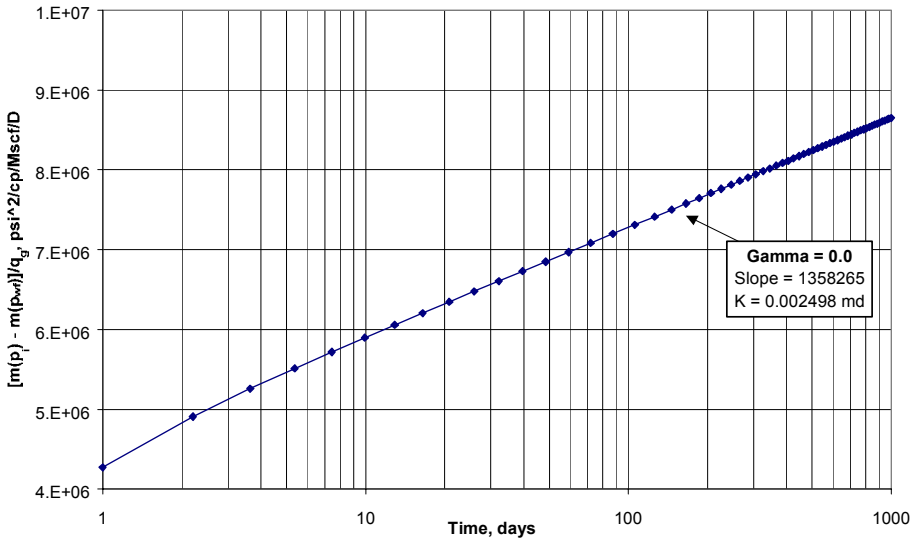

Fig. 4.8- Constant permeability case of $m(p_i)$-$m(p_{wf})/q_g$ as a function of time for an infinite acting reservoir producing at constant q_g.

Next, pressure-dependent permeability was simulated. Fig. 4.9 shows that for each value of permeability modulus, a semi-log straight-line is observed. This confirms that the reservoir is infinite acting (transient).

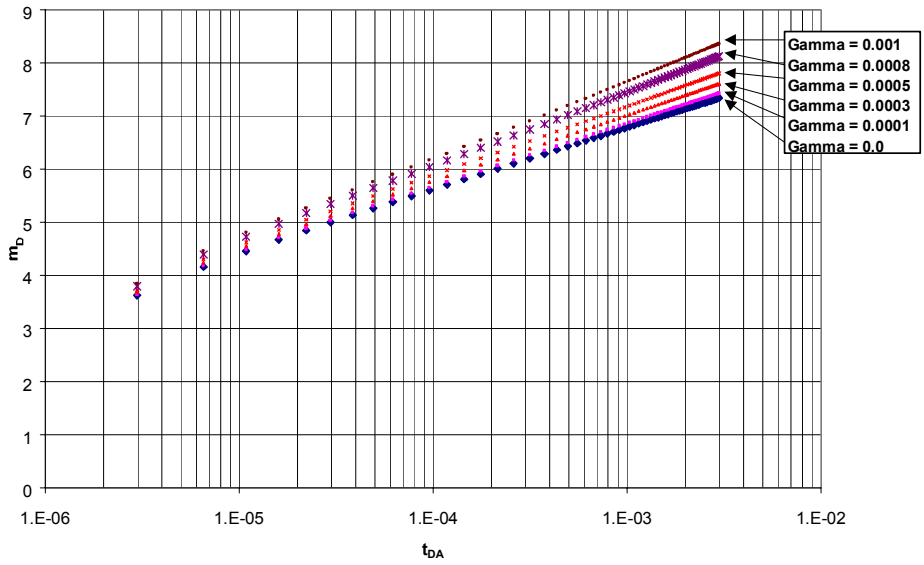

Fig. 4.9- Effect of pressure-dependent permeability for an infinite acting reservoir producing at constant q_g.

Fig. 4.10 shows the results for the same six permeability modulus values. For each permeability modulus value, different permeabilities were calculated.

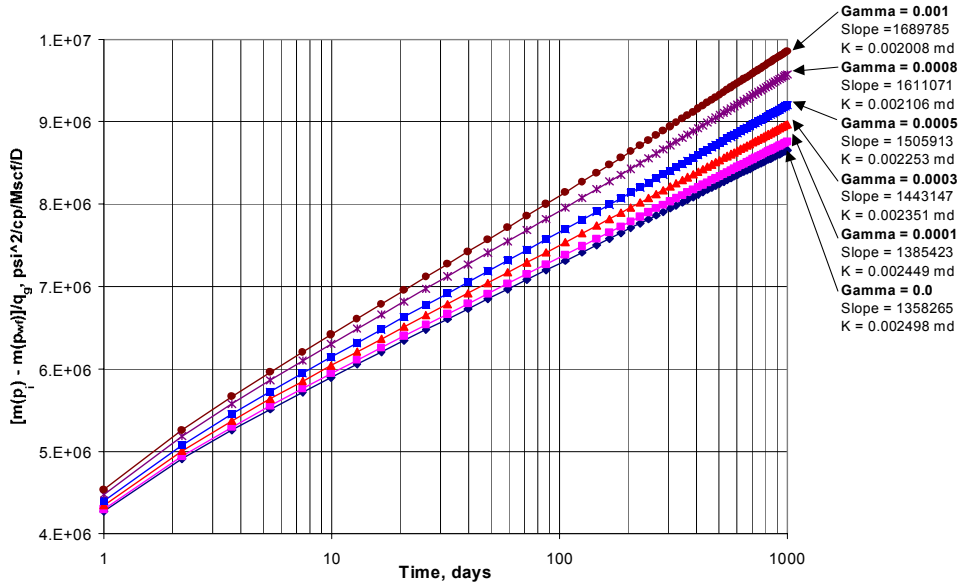

Fig. 4.10- Comparison of $m(p_i)$-$m(p_{wf})/q_g$ as a function of time for an infinite acting reservoir producing at constant q_g.

Fig. 4.11 shows the calculated permeability variation as a function of permeability modulus.

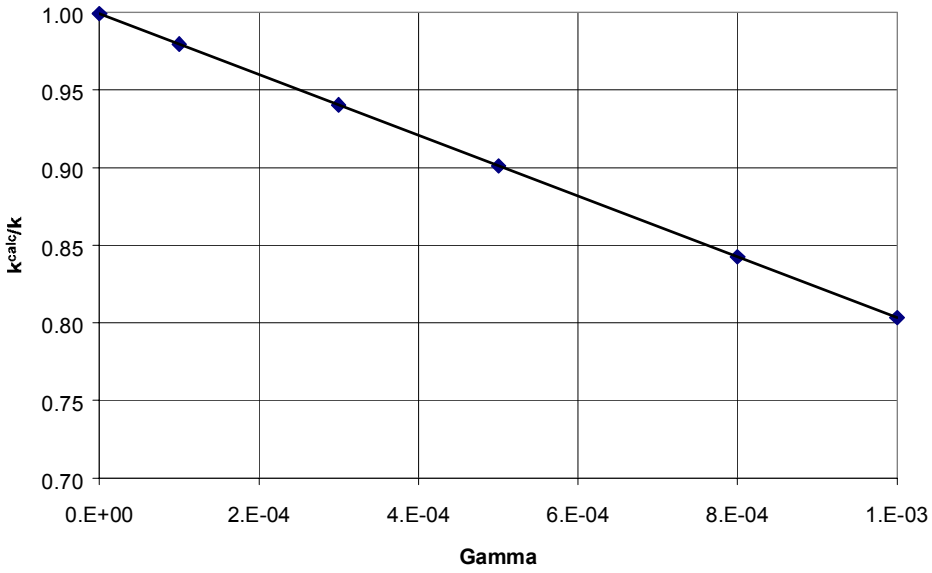

Fig. 4.11- Permeability ratio calculated on transient period versus permeability modulus for Simulation Case 2 and constant q_g.

Fig. 4.12 shows the skin values due to permeability reduction calculated from the intercept of each semi-log straight versus permeability modulus plot in Fig. 4.10. These values should be verified, due to the unexpected negative result obtained for this case.

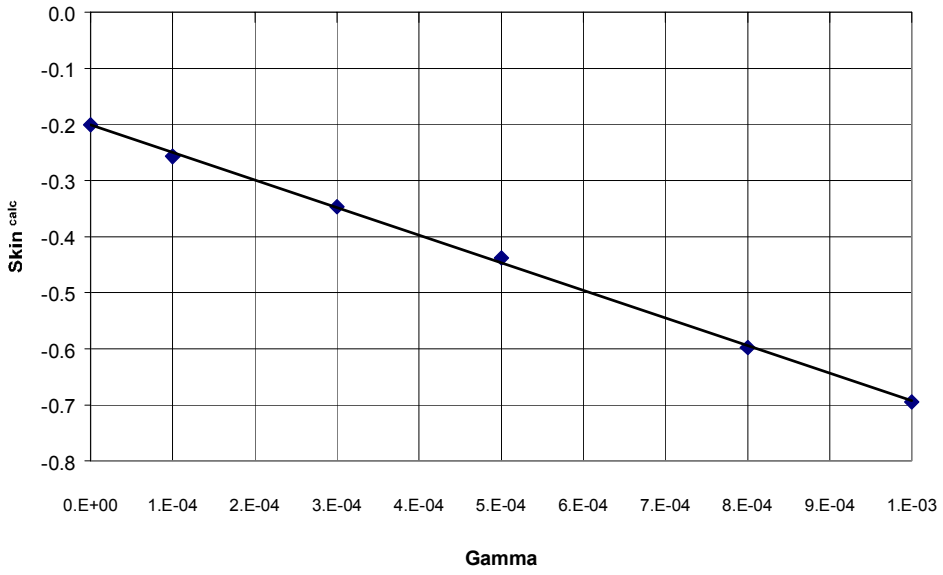

Fig. 4.12- Calculated skin versus permeability modulus for Simulation Case 2 (constant q_q).

4.3 Simulation Case 3: Finite Acting – Constant p_{wf}

This is a radial flow case where the well in located in the center of the reservoir. It is finite acting (closed reservoir boundary), and the bottom-hole pressure is kept constant at 50 psi. Table 4.3 summarizes other characteristics of the reservoir.

Table 4.3- Main Characteristics of the Reservoir – Simulation Case 3.

Reservoir characteristic	Values
Initial porosity	15%
Initial reservoir pressure	8,800 psi
Initial permeability	0.025 md
Initial total compressibility	3.49E-5 1/psi
Reservoir temperature	750 °R
Bottom-hole pressure	50 psi
Reservoir thickness	362 ft

Fig. 4.13 shows both transient flow and boundary dominated flow for constant permeability ($\gamma = 0$). The end of the transient flow period is also shown.

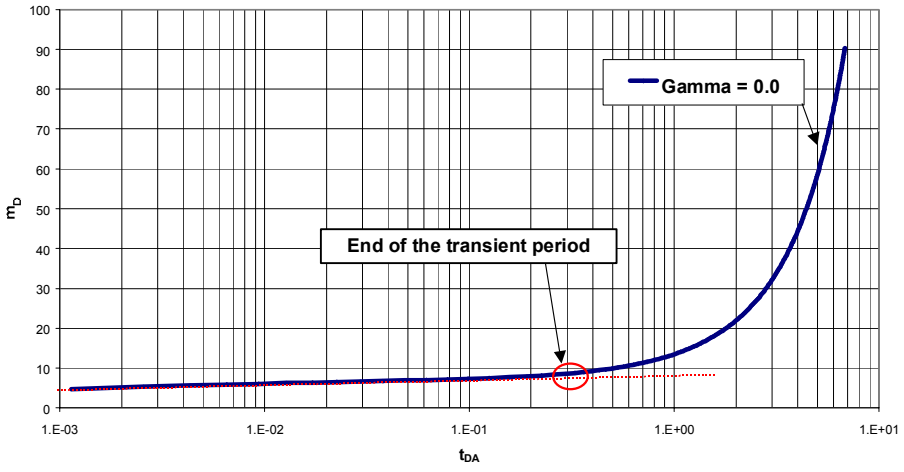

Fig. 4.13- Constant permeability case of m_D as a function of t_{DA} for a finite acting reservoir producing at constant p_{wf}.

Superposition time has been used as a tool to analyze variable flow rate[31,32] without knowing the average reservoir pressure. Superposition time is defined as: (Ibrahim *et al.*[28])

$$\frac{\left[m(p_i)-m(p_{wf})\right]}{q_{gm}}=\tilde{m}_{pss}\left[\sum_{i=1}^{m}\frac{\Delta q_{gi}}{\Delta q_{gm}}\left(t_m-t_{i-1}\right)\right]+b \quad \text{.....(4.3)}$$

The slope (Ibrahim *et al.*[28], $\tilde{m}_{pss}$) from plotting $[m(p_i)-m(p_{wf})]/q_g$ versus Superposition time was used to determine the OGIP as:

$$OGIP=\frac{2p_iS_{gi}}{Z_i(\mu_g c_t)_i}\left(\frac{1}{\tilde{m}_{PSS}}\right) \quad \text{.....(4.4)}$$

Fig. 4.14 shows $[m(p_i)-m(p_{wf})]/q_g$ versus superposition time (Super-t) taking into account the rate change but it does not correct for pressure-dependent gas properties. Therefore there is no unique value of *OGIP* from the Superposition time plot.

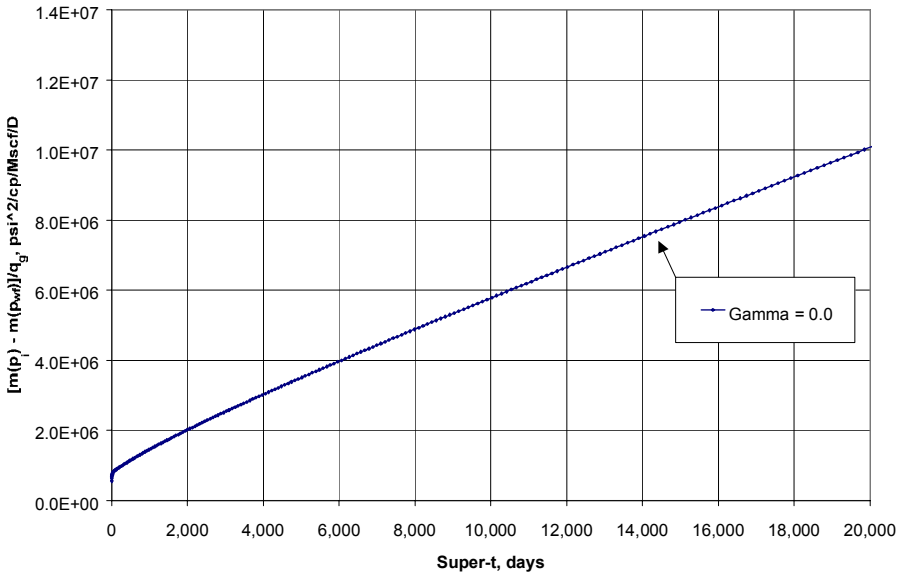

Fig. 4.14 Constant permeability case of $m(p_i)-m(p_{wf})/q_g$ as a function of Superposition time for a finite acting reservoir producing at constant p_{wf}.

Next, pressure-dependent permeability was included. Fig. 4.15 shows the transition between transient flow and boundary-dominated flow (diagonal line). It is important to see the different times to reach boundary dominated flow for each permeability modulus value. When the permeability modulus value increases, the time to reach boundary-dominated flow increases due to decreasing permeability.

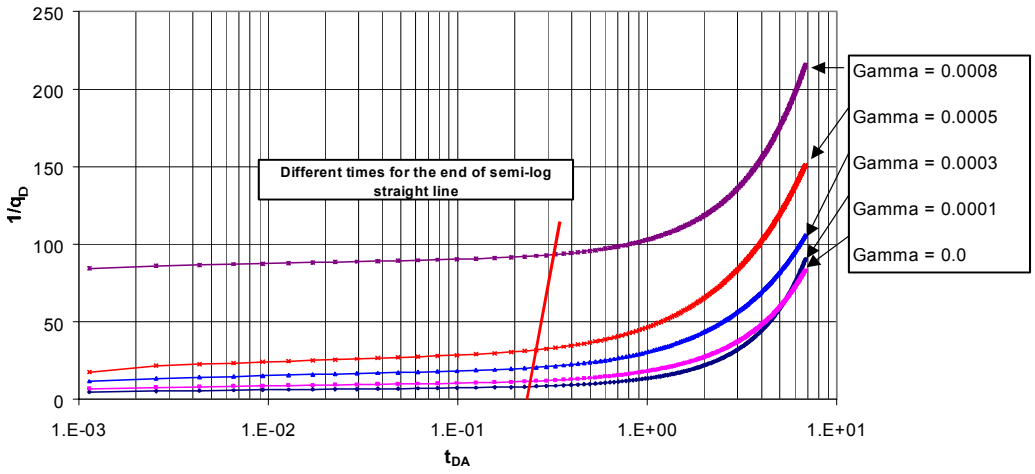

Fig. 4.15- Effect of pressure-dependent permeability for a finite acting reservoir producing at constant p_{wf}. Diagonal line shows end of transient period for each permeability modulus.

Fig. 4.16 shows non-linearity during boundary-dominated flow. This non-linearity is due non-constant diffusivity. In order to get the best estimate of *OGIP* for each permeability modulus, the tangent slope at the end of the transient period was used for each case, following the procedure recommended by Ibrahim *et al.*[28] and Wattenbarger *et al.*[32] For each permeability modulus a different estimated *OGIP* value is calculated. See Appendix B for calculation details.

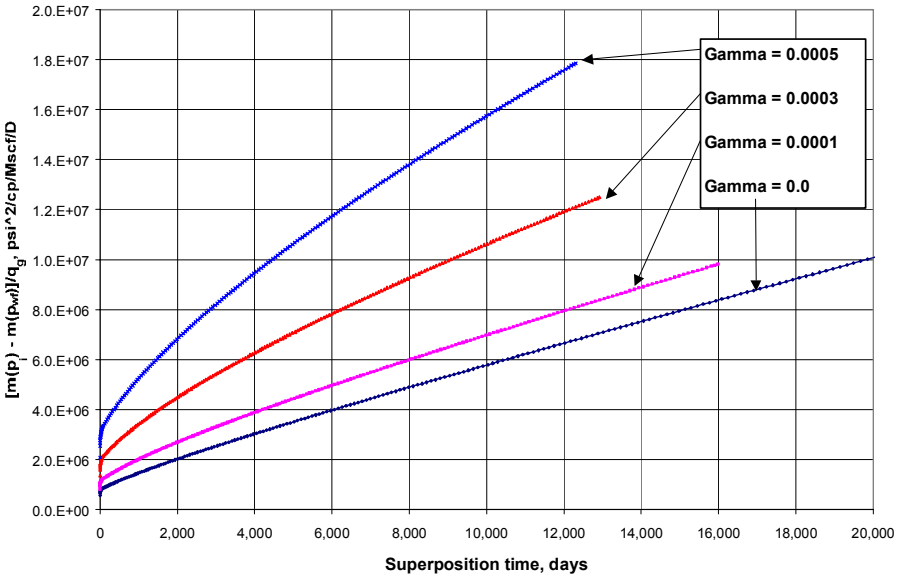

Fig. 4.16- $m(p_i)$-$m(p_{wf})/q_g$ as a function of Superposition time for a finite acting reservoir producing at constant p_{wf}.

Fig. 4.17 shows the ratio of calculated *OGIP* to true *OGIP* for each permeability modulus value from Simulation Case 3. From this plot can be concluded that the Ibrahim *et al*.[28] method underestimates the *OGIP* value for tight gas reservoirs with pressure-dependent permeability.

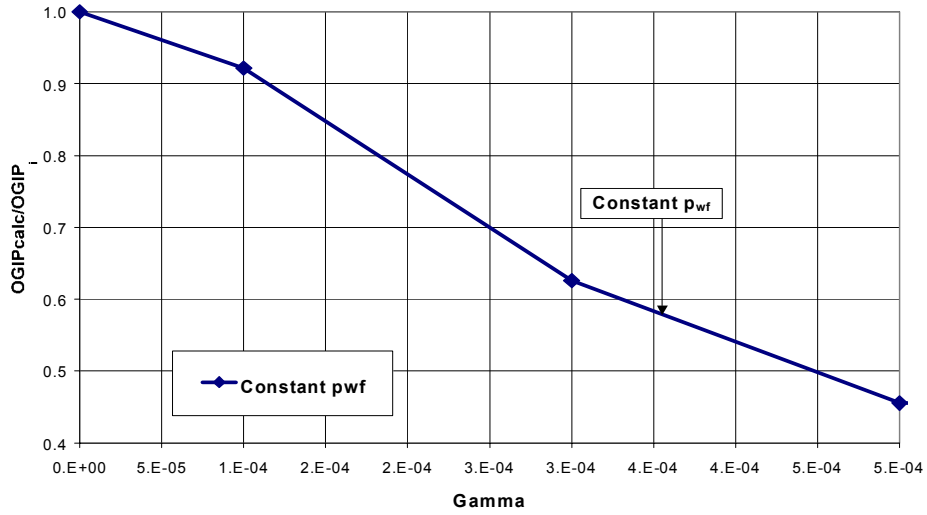

Fig. 4.17- *OGIP* ratio versus permeability modulus for a finite acting reservoir producing at constant p_{wf}.

For each permeability modulus in Simulation Case 3, different productivity index values are calculated (at the end of transient period). Fig. 4.18 shows how the productivity index decreases when permeability modulus increases. For the purpose of this work, the productivity index is defined as:

$$J = \frac{q_g}{\left[m(\bar{p}) - m(p_{wf})\right]} \quad \text{.....(4.5)}$$

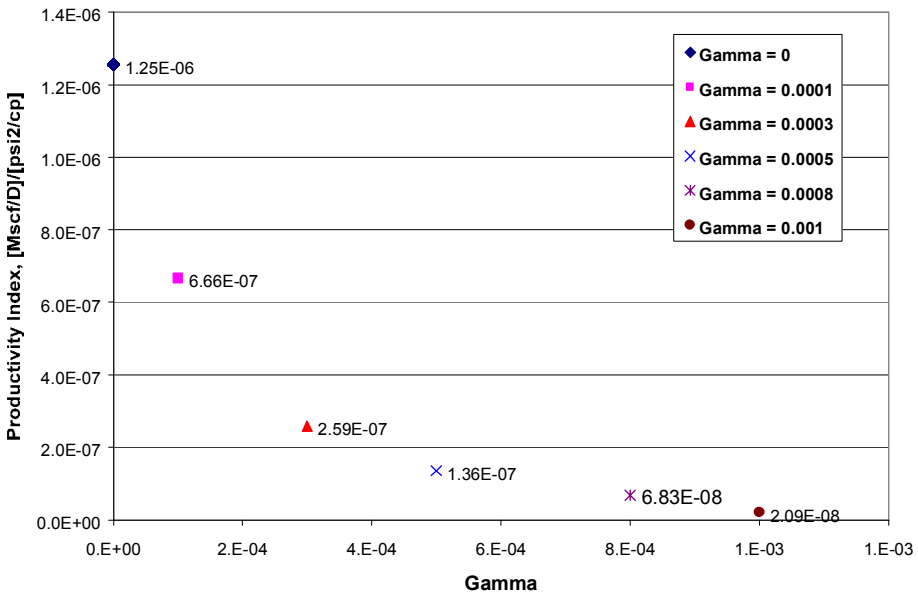

Fig. 4.18- Productivity index as a function of permeability modulus for a finite acting reservoir producing at constant p_{wf}.

4.4 Simulation Case 4: Finite Acting – Constant q_g

This is a radial flow case with the well in located in the center of the reservoir. It is finite acting (closed reservoir boundary) and the gas production rate is constant at 300 Mscf/D. Table 4.4 summarizes other characteristics of the reservoir (see Appendix A for GASSIM data file).

Table 4.4- Main Characteristics of the Reservoir - Simulation Case 4.

Reservoir characteristic	Values
Initial porosity	15%
Initial reservoir pressure	8,800 psi
Initial permeability	0.025 md
Initial total compressibility	3.49E-5 1/psi
Reservoir temperature	750 °R
Gas production rate	300 Mscf/D
Reservoir thickness	362 ft

Fig. 4.19 shows the end of the semi-log straight line for constant permeability ($\gamma = 0$).

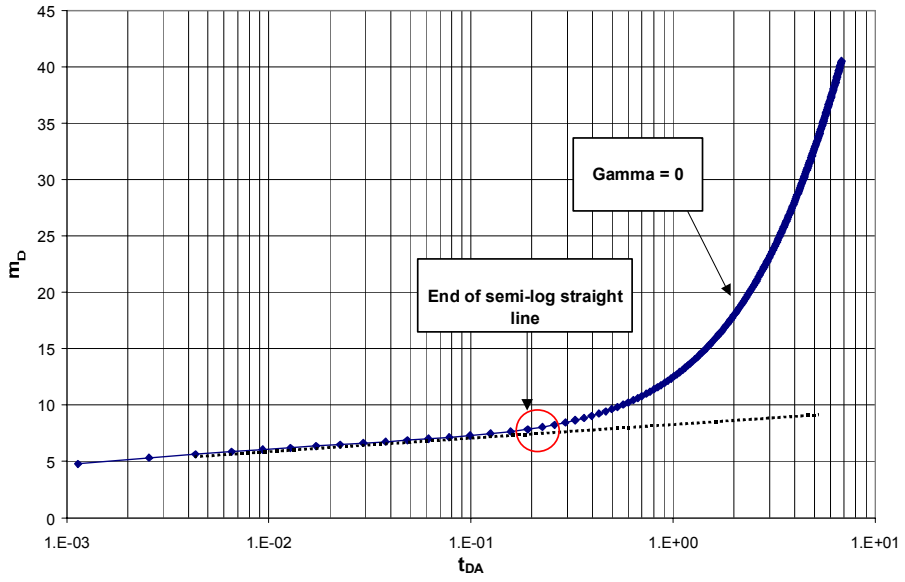

Fig. 4.19- Constant permeability case of m_D as a function of t_{DA} for a finite acting reservoir producing at constant q_g. Shows the end of semi-log straight line.

Fig. 4.20 shows non-linearity during the *PSS* period (constant permeability). This non-linearity is due to pressure dependent fluid and rock properties. In order to get the best *OGIP* estimate, the slope at the end of the transient period was used. See Appendix B for details.

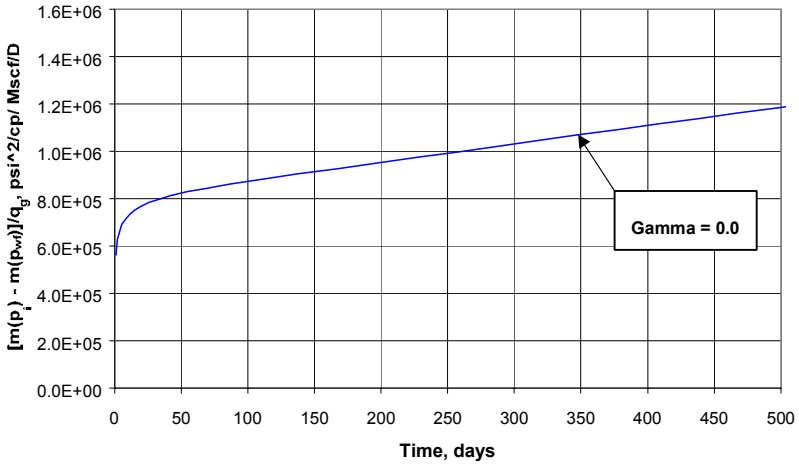

Fig. 4.20- Constant permeability case of $m(p_i)-m(p_{wf})/q_g$ as a function of time for a finite acting reservoir producing at constant q_g.

Next, the effect of pressure-dependent permeability was studied. Fig. 4.21 shows the end of the transient period. Although it is difficult to see in this plot, it is important to note that for each permeability modulus a different time to reach *PSS* is observed. When the permeability modulus value increases, the time to reach *PSS* increases. For case 4, only three permeability modulus values where analyzed due to convergence problems with GASSIM at higher values of permeability modulus.

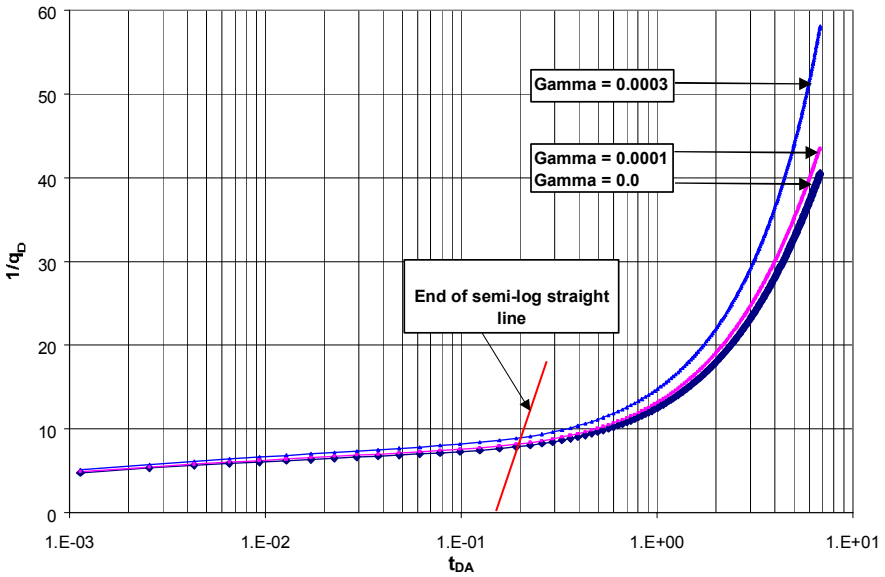

Fig. 4.21- Comparison of $1/q_D$ as a function of t_{DA} for a finite acting reservoir producing at constant q_g.

In Fig. 4.22 the slope fof the plot of $m(p_i)$-$m(p_{wf})/q_g$ versus time at the end of transient flow gives the most accurate estimates of *OGIP*. For each permeability modulus value a different values of *OGIP* is calculated.

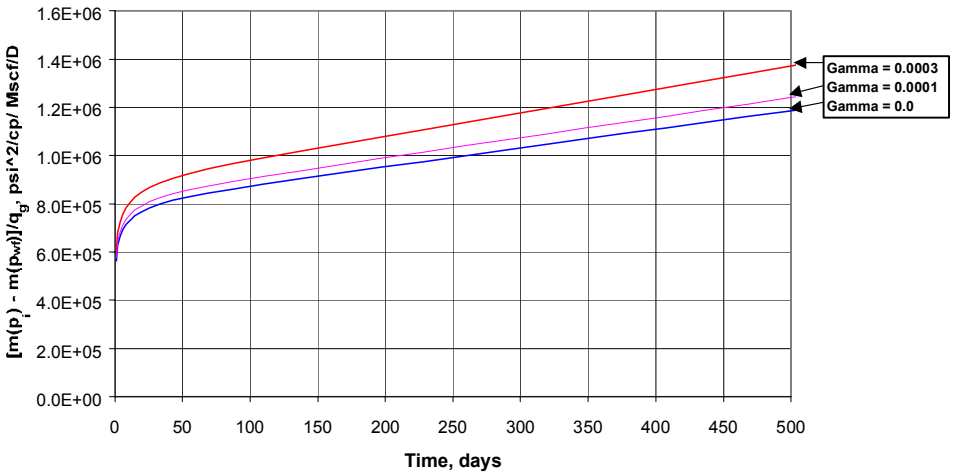

Fig. 4.22- $m(p_i)$-$m(p_{wf})/q_g$ as a function of time for a finite acting reservoir producing at constant q_g.

Fig. 4.23 shows how the behavior calculated *OGIP* behave for the permeability modulus values simulated in Case 4. There is no unique *OGIP* value and the method of Ibrahim *et al.*[28] underestimates *OGIP* for tight gas reservoirs with pressure-dependent permeability.

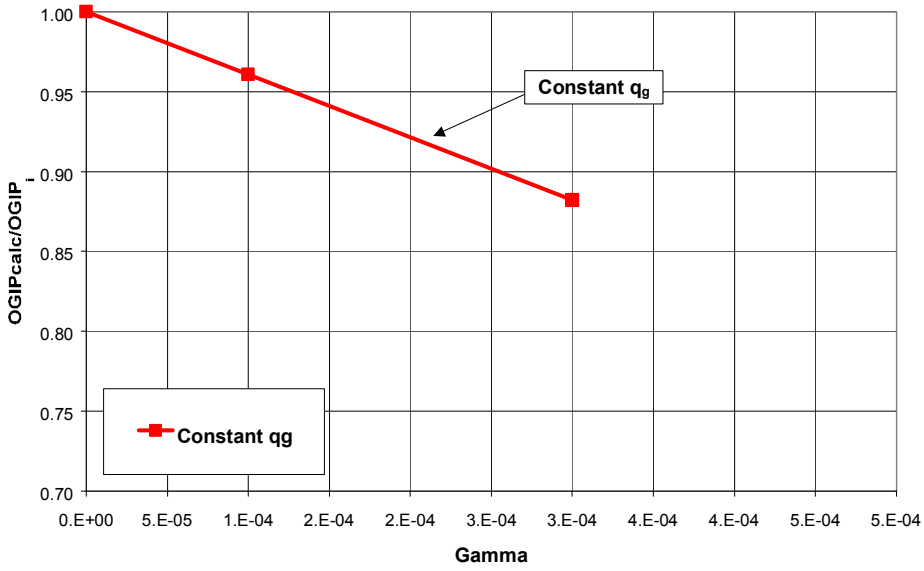

Fig. 4.23- *OGIP* ratio versus permeability modulus for a finite acting reservoir producing at constant q_g.

For each permeability modulus value in Simulation Case 4 (constant q_g), different values of productivity index are also calculated. Fig. 4.24 shows how the productivity index decreases when permeability modulus increases for Case 4.

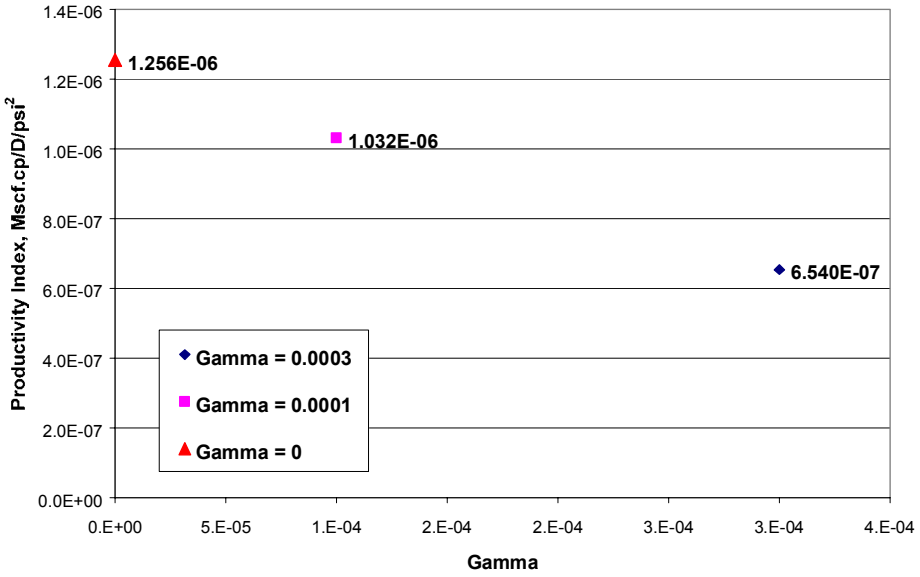

Fig. 4.24- Productivity index versus permeability modulus for a finite acting reservoir producing at constant q_g.

4.5 Summary

Based on the simulation cases studied, several interesting observation follows: 1) When we consider the effect of pressure-dependence permeability, we calculated different permeability values for each permeability modulus. 2) From the closed reservoir cases analyzed in this work, we obtain different calculated *OGIP* values for each permeability modulus.

This means that stress sensitivity in a tight gas reservoir simulation is significant and needs to be taken into account.

Fig. 4.25 shows the ratio of calculated permeability to initial permeability for Simulation Case 1 (constant p_{wf}) and Case 2 (constant q_g) in the same plot. It should be noted that the drawdown for Case 1 was approximately 4800 psia, while the drawdown for Case 2 (constant q_g) was approximately 250 psia.

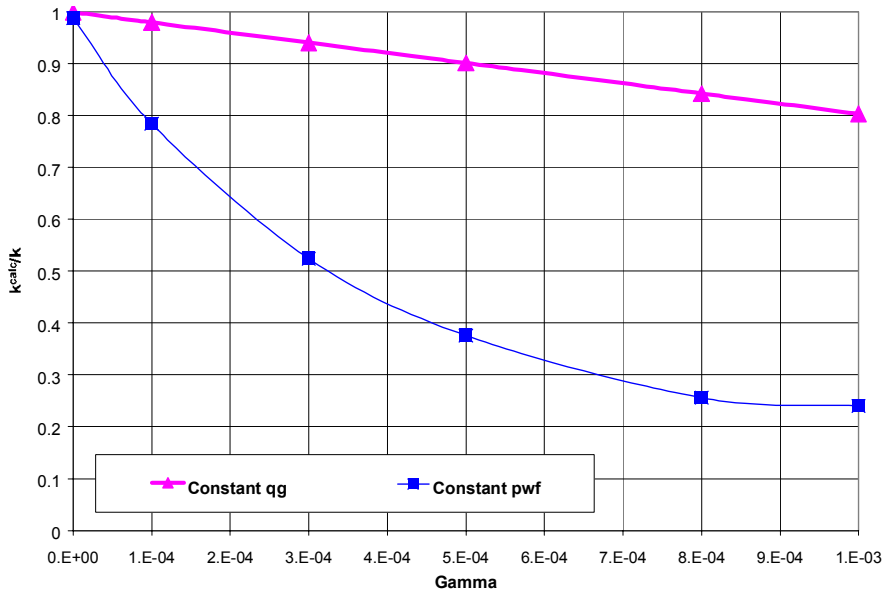

Fig. 4.25- Permeability ratios for constant p_{wf} and constant q_g versus permeability modulus.

Fig. 4.26 shows the skin values for constant p_{wf} and constant q_g cases, versus permeability modulus. Fig. 4.27 shows the *OGIP* ratios for constant p_{wf} and constant q_g cases, versus permeability modulus. It should be noted that the drawdown for the cases was different.

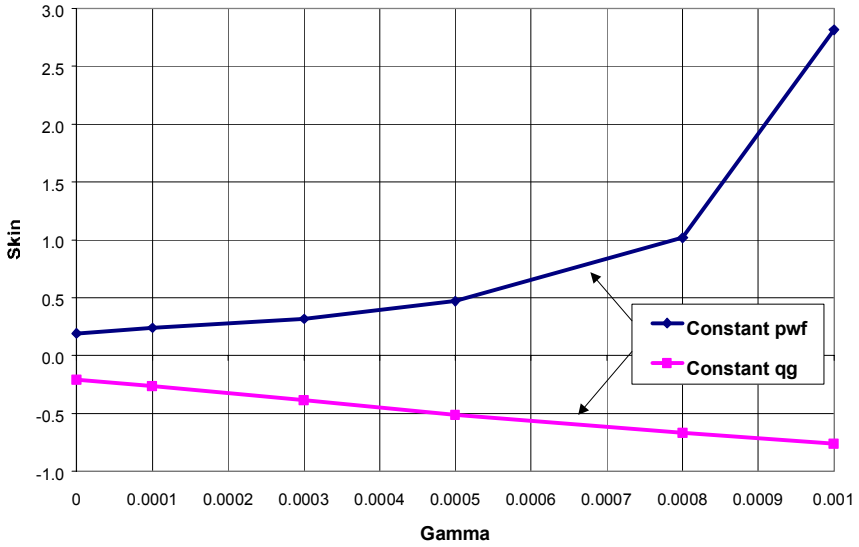

Fig. 4.26- Calculated skin values versus permeability modulus.

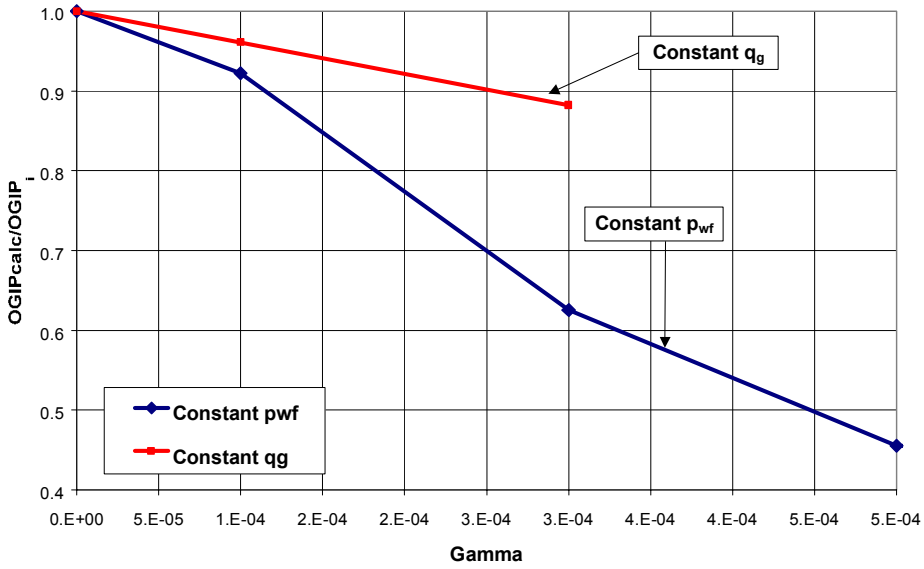

Fig. 4.27- *OGIP* ratios versus permeability modulus for both constant p_{wf} and q_g.

CHAPTER V

CONCLUSIONS

Large quantities of gas have yet to be discovered and produced from tight gas reservoirs where pressure-dependent permeability is likely to be significant. Based upon work performed for this thesis the following conclusions were drawn.

1. Based on field production data it is not possible to determine the correct permeability value for tight gas reservoirs with pressure-dependent permeability. For all permeability modulus values studied, semi-log transient, straight lines were obtained and it is impossible to distinguish between constant permeability and pressure-dependent permeability.

2. Productivity index (at the end of the transient period) decreases when permeability modulus increases. Dimensionless skin factor increases when permeability modulus increases.

3. The method of Ibrahim e*t al*.[28] under estimates *OGIP* for tight gas reservoirs with pressure-dependent permeability. The most favorable case was used, taking the slope at the end of the transient period.

NOMENCLATURE

B = formation volume factor, rcf/scf
c = fluid compressibility, 1/psi
c_f = rock compressibility, 1/psi
c_t = total system compressibility, 1/psi
E = modulus of elasticity of bulk, psi
E_i = modulus of elasticity of rock matrix, psi
G = shear modulus, psi
J_g = gas productivity index, Mscf.cp/D/psi^2
k = permeability, md
M = molecular mass, kg
$m(p)$ = real gas pseudo pressure, psi^2/cp
$m(p\_bar) = m(p)$ at average reservoir pressure, psi^2/cp
$m(p_i) = m(p)$ at initial pressure, psi^2/cp
$m(p_{wf}) = m(p)$ at flowing wellbore pressure, psi^2/cp
$OGIP$ = Original Gas in Place, m^3, scf
p = pore pressure, psia
p_bar = average reservoir pressure, psi
p_D = dimensionless pressure
p_d = drainage boundary pressure, psia
p_o = initial pore pressure, psia
PSS = pseudo-steady state
p_{wf} = bottom-hole pressure, psi
q_g = gas flow rate, Mscf/D
r = radial distance from center of well, ft
r_d = drainage boundary radius, ft
r_w = wellbore radius, ft
T = temperature, °C
t_D = dimensionless time
z = gas compressibility factor
Z = gas deviation factor
$Z(p)$ = gas deviation factor, a function of pressure at constant temperature.
ϕ = porosity
μ = viscosity, cp
ρ = fluid density, lb$_m$/ft^3
∇ = gradient
σ = macrostress, psi
ε = normal strain

γ = permeability modulus
ν = Poisson's ratio of bulk sample
β = ratio of compressibility of rock matrix to that of the bulk
τ = shear stress, psi
$\nabla\bullet$ = divergence
$\mu(p)$ = viscosity a function of pressure, cp
σ' = microstress, psi
σ'' = effective microstress, psi
σ''' = effective macrostress, psi
∇^2 = Laplacian operator
σ_c = confining pressure on core, psi
σ_f = stress due to horizontal loading, psi
ν_l = Poisson's ratio of rock matrix
σ_o = stress due to overburden, psi
$\tilde{m}(p_{PSS})$ = Cartesian slope of $m(p_i)$-$m(p_{wf})/q_g$ versus Superposition time, psi^2/cp
$\vec{u}$ = Darcy velocity, ft/D
$\tilde{m}(p)$ = Modified gas pseudo pressure considering $k(p)$, md*psia^2/cp

Subscripts

A = area
$calc$ = calculated
D = dimensionless
g = gas
i = initial
r = radial
z = vertical
θ = tangential

REFERENCES

1. Vairogs, J., Hearn, C. L., Dareing, D. W., and Rhoades, V. W.: "Effect of Rock Stress on Gas Production From Low-Permeability Reservoirs," *JPT* (September 1971) 1161-67; *Trans*., AIME, **251**.

2. Vairogs, J. and Rhoades, V. W.: "Pressure Transient Test in Formations Having Stress-Sensitive Permeability," *JPT* (August 1973) 965-70; *Trans*., AIME, **255**.

3. Ostensen, R. W.: "The Effect of Stress-Dependent Permeability on Gas Production and Well Testing," *SPEFE* (June 1986) 227-35; *Trans*., AIME **284**.

4. Raghavan, R., Scorer, J. D. T., and Miller, F. G.: "An Investigation by Numerical Methods of the Effect of Pressure-Dependent Rock and Fluid Properties on Well Flow Tests," *SPEJ* (June 1972) 267-75; *Trans*., AIME **253**.

5. Samaniego-V, F., Brigham, W. E., and Miller, F. G.: "An Investigation of Transient Flow of Reservoir Fluids Considering Pressure-Dependent Rock and Fluid Properties," *SPEJ* (April 1977) 140-50; *Trans*., AIME **263**.

6. Fatt, I.: "Pore Volume Compressibility of Sandstone Reservoir Rocks," (January 1958) 362-64 *Trans*., AIME **213**.

7. Gray, D. H., Fatt, I., and Bergamini, G.: "The Effect of Stress on Permeability of Sandstone Cores," *SPEJ* (June 1963) 95-100; *Trans*., AIME **228**.

8. McLatchie, A. S., Hemstock, R. A., and Young, J. W.: "The Effective Compressibility of Reservoir Rock and Its Effects on Permeability," (September 1958) 386-388 *Trans*., AIME **213**.

9. Brower, K. R., and Morrow, N. R.: "Fluid Flow in Cracks as Related to Low-Permeability Gas Sands," paper SPE 11623 presented at the 1983 SPE/DOE Symposium on Low Permeability, Denver, 14-16 March.

10. Pinzon, C. L., Chen, H., and Teufel, L. W.: "Complexity of Well Testing Analysis of Naturally-Fractured Gas-Condensate Wells in Colombia," paper SPE 59013 presented at the 2000 SPE International Petroleum Conference and Exhibition, Mexico City, 1-3 February.

11. Jelmert, T. A., and Selseng, H.: "Pressure *Trans*ient Behavior of Stress-Sensitive Reservoirs," paper SPE 38970 presented at the 1997 SPE Latin American/Caribbean Petroleum Engineering Conference, Rio De Janeiro, Brazil, 30 Aug. –3 Sept.

12. Kikani, J., and Pedrosa, O. A.: "Perturbation Analysis of Stress-Sensitive Reservoirs," paper SPE 20053 presented at the 1990 SPEFE California Regional Meeting, Ventura, 4-6 April.

13. Pedrosa, O. A. Jr.: "Pressure Transient Response in Stress-Sensitive Formations," paper SPE 15115 presented at the 1986 SPE California Regional Meeting, Oklahoma City, 2-4 April.

14. Al-Hussainy, R., Ramey, H. J., and Crawford, P. B.: "The Flow of real gases Through Porous media," (May 1966), 624-636; *Trans*., AIME **237**.

15. Fatt. I. And Davis, T. H.: "The reduction in Permeability with Overburden Pressure," (1952), 329; *Trans*., AIME **195**.

16. Fatt, I.: "The effect of Overburden Pressure on Relative Permeability," (1953), 325-326; *Trans*., AIME **198**.

17. Wyble, D. O.: "Effect of Applied Pressure on Conductivity, Porosity and Permeability of Sandstones," (1958) 430-432; *Trans*., AIME **213**.

18. Deily, F. H. and Owens, F. C.: "Stress Around a Wellbore," paper SPE 2557 presented at the 1969 SPE 44th Annual Fall Meeting, Denver, 28 September - 1 October.

19. Lubinski, A.: "The Theory of Elasticity for Porous Bodies Displaying a Strong Pore Structure," *Proc*., Second U.S. National Congress of Applied Mechanics, University of Michigan, Ann Arbor, MI (1954) 247-256.

20. Ostensen, R. W.: "Microcrack Permeability in Tight Gas Sandstone," *SPEJ* (December 1983) 919-927.

21. Jones, F. O. and Owens, W. W.: "A Laboratory Study of Low-Permeability Gas Sands," *JPT* (September 1980) 1631-1640.

22. Chin, L. Y., Raghavan, R., and Thomas, L. K.: "Fully Coupled Analysis of Well Responses in Stress-Sensitive Reservoirs," paper SPE 48967 presented at the SPE Annual Technical Conference & Exhibition, New Orleans, Louisiana, 27-30 September, 1998.

23. Samaniego-V, F., Brigham, W. E., and Miller, F. G.: "Performance-Prediction Procedure for Transient Flow of Fluids Through Pressure-Sensitive Formations," paper SPE 6051 presented at the SPE-AIME 51st Annual Fall Technical Conference & Exhibition, New Orleans, 3-6 October, 1976.

24. Samaniego, F. and Cinco-Ley, H.: "On the Determination of the Pressure-Dependent Characteristics of a Reservoir Through Transient Pressure Testing," paper SPE 19774, presented at the 1989 SPE Annual Technical Conference and Exhibition, San Antonio, Texas, 8-11 October.

25. Warren, J.E. and Price, H.S.: "Flow in Heterogeneous Porous Media," *SPEJ* (Sept. 1961) 153-169.

26. Thomas, R. D. and Ward, D. C.: "Effect of Overburden Pressure and Water Saturation on Gas Permeability of Tight Sandstone Cores," *JPT* (February 1972) 120-124.

27. Wattenbarger, R. A., El-Banbi A. H., Villegas M. E. and Maggard, J. B.: "Productivity Analysis of Linear Flow Into Fractured Tight Gas Wells," paper SPE 39931, presented at the 1998 SPE Rocky Mountain Regional/Low-Permeability Reservoirs Symposium and Exhibition, Denver, Colorado, 5-8 April.

28. Ibrahim, M., Wattenbarger, R. A., and Helmy, W.: "Determination of *OGIP* for Wells in Pseudosteady-State-Old Techniques, New Approaches," paper SPE 84286, presented at the 2003 SPE Annual Technical Conference and Exhibition, Denver, Colorado, 5-8 October.

29. Matthews, C. S., and Russell, D. G.: "Pressure Buildup and Flow Test in Wells," Society of Petroleum Engineers, Monograph Series, New York, Dallas, (1967) 7.

30. Nur, A., and Yilmaz, O.: "Pore Pressure in Fronts in Fractured Rock Systems," Dissertation, Dep. of Geophysics, Stanford U., Stanford, CA (1985).

31. Arevalo-Villagran, J. A., Wattenbarger, R. A., Samaniego-Verduzco, F., and Pham, T. T.: "Prosuction Analysis of Long-Term Linear Flow in Tight Gas Reservoirs: Case Histories," paper SPE 71516 presented at the 2001 Annual Technical Conference and Exhibition, New Orleans, LA, 30 September -3 October.

32. Ibrahim, M., and Wattenbarger, R. A.: "Relationship between Superposition Time and Material Balance Time in *PSS*," report for the Reservoir Modeling Consortium, Texas A&M University, September, 2002.

33. Lee, W. J., and Wattenbarger, R. A.: Gas Reservoir Engineering, SPE Textbook Series, Richardson, Texas, Vol. 5, 1996

APPENDIX A

GASSIM Data Files

Simulation Case 1: Infinite Acting – Constant p_{wf}

```
CMNT    Radial case, constant pwf for gas well
CMNT    Single    Value     Data
CMNT
IMAX          53
JMAX           1
RWEL        0.25
CROC    4.08E-06
GRAV       0.717
PREF        8800
TSC          520
PSC        14.65
T            750
NEWT           4
BETA           0
TABL           0
IMAP           1
SWAT        0.47
CWAT     4.1E-06
GAMMA       0.001
END
CMNT
CMNT    Grid      Data
CMNT
KX          0.0025
KY          0.0025
PHI           0.15
POI           8800
CMNT
RR             -1
               0.30      0.36      0.43      0.51      0.61      0.72      0.86      1.03      1.23      1.47
               1.76      2.10      2.50      2.99      3.57      4.26      5.09      6.07      7.25      8.65
              10.33     12.34     14.73     17.58     20.99     25.06     29.92     35.73     42.65     50.92
              60.80     72.58     86.66    103.46    123.52    147.47    176.06    210.20    250.96    299.62
             357.71    427.07    509.88    608.74    726.77    867.68   1035.92   1236.78   1476.59   1762.89
            2104.70   2512.79   3000.00
CMNT
DELY        361.99
END
CMNT    Schedule  Data
PMAP           2
PLOT           2
DIMP           0
NAME           1         1         1         0
ALPH         1.2
DELT           1
DTMX          20
PWF            1      4000
TIME        1000
END
```

Simulation Case 2: Infinite Acting – Constant q_g

```
CMNT    Radial case, constant qg for gas well
CMNT    Single    Value     Data
CMNT
IMAX          53
JMAX           1
RWEL        0.25
CROC    4.08E-06
GRAV       0.717
PREF        8800
TSC          520
PSC        14.65
T            750
NEWT           4
BETA           0
TABL           0
IMAP           1
SWAT        0.47
CWAT     4.1E-06
GAMMA      0.001
END
CMNT
CMNT    Grid      Data
CMNT
KX         0.0025
KY         0.0025
PHI          0.15
POI          8800
CMNT
RR            -1
              0.30      0.36      0.43      0.51      0.61      0.72      0.86      1.03      1.23      1.47
              1.76      2.10      2.50      2.99      3.57      4.26      5.09      6.07      7.25      8.65
             10.33     12.34     14.73     17.58     20.99     25.06     29.92     35.73     42.65     50.92
             60.80     72.58     86.66    103.46    123.52    147.47    176.06    210.20    250.96    299.62
            357.71    427.07    509.88    608.74    726.77    867.68   1035.92   1236.78   1476.59   1762.89
           2104.70   2512.79   3000.00
CMNT
DELY        361.99
END
CMNT    Schedule  Data
PMAP           2
PLOT           2
DIMP           0
NAME           1         1         1         0
ALPH         1.2
DELT           1
DTMX          20
QG             1     10000
TIME        1000
END
```

Simulation Case 3: Finite Acting – Constant p_{wf}

```
CMNT      Radial case, constant pwf for gas well
CMNT
CMNT      Single      Value       Data
CMNT
IMAX            53
JMAX             1
RWEL          0.25
CROC      4.08E-06
GRAV         0.717
PREF          8800
TSC            520
PSC          14.65
T              750
NEWT             4
BETA             0
TABL             0
IMAP             1
SWAT          0.47
CWAT      4.1E-06
GAMMA        0.0003
END
CMNT      Grid        Data
KX            0.025
KY            0.025
PHI            0.15
POI            8800
CMNT
RR               -1
          0.288552  0.333048  0.384407  0.443685  0.512104  0.591074  0.682221  0.787424   0.90885  1.049001
          1.210764  1.397472  1.612971  1.861702  2.148789  2.480147  2.862602  3.304034  3.813538  4.401611
          5.080369  5.863796  6.768033  7.811709  9.016326   10.4067  12.01149  13.86374  16.00162  18.46918
          21.31725  24.60451  28.39869  32.77796  37.83254  43.66657  50.40024   58.1723  67.14286  77.49673
          89.44725  103.2406   119.161  137.5364  158.7455  183.2251  211.4796  244.0912  281.7317  325.1766
           375.321   433.198       500
DELY          361.99
END
CMNT      Schedule    Data
CMNT
PMAP             2
PLOT             2
DIMP             0
NAME             1         1         1         0
ALPH          1.25
DELT             1
DTMX            30
PWF              1        50
TIME          6000
END
```

Simulation Case 4: Finite Acting – Constant q_g

```
CMNT      Radial case, constant qg for gas well
CMNT
CMNT      Single      Value    Data
CMNT
IMAX            53
JMAX             1
RWEL          0.25
CROC      4.08E-06
GRAV         0.717
PREF          8800
TSC            520
PSC          14.65
T              750
NEWT             4
BETA             0
TABL             0
IMAP             1
SWAT          0.47
CWAT       4.1E-06
GAMMA            0
END
CMNT      Grid        Data
KX            0.025
KY            0.025
PHI            0.15
POI            8800
CMNT
RR               -1
                0.29    0.33    0.38    0.44    0.51    0.59    0.68    0.79    0.91    1.05
                1.21    1.40    1.61    1.86    2.15    2.48    2.86    3.30    3.81    4.40
                5.08    5.86    6.77    7.81    9.02   10.41   12.01   13.86   16.00   18.47
               21.32   24.60   28.40   32.78   37.83   43.67   50.40   58.17   67.14   77.50
               89.45  103.24  119.16  137.54  158.75  183.23  211.48  244.09  281.73  325.18
              375.32  433.20  500.00
CMNT
DELY          361.99
END
CMNT      Schedule  Data
PMAP             2
PLOT             2
DIMP             0
NAME             1       1       1       0
ALPH          1.25
DELT             1
DTMX            30
QG               1  300000
TIME          6000
END
```

APPENDIX B

Permeability calculations

Calculated the permeability values from Fig. 4.5 and Fig. 4.11 used the analytical pseudo-pressure equation (equation B1) for the transient period and the slope (equation B5) of plotting $m(p_i)$-$m(p_{wf})/q_g$ versus log time, to calculate the permeability values.

$$m_D = \frac{1}{2}\ln t_D + 0.4045 + S \quad \text{.....(B1)}$$

$$\text{where} \quad t_D = \frac{0.00633kt}{\phi\mu c_t rw^2} \text{ , ...(B2)}$$

$$m_D = \frac{kh[m(p_i) - m(p_{wf})]}{1422 q_g T} \text{.....(B3)}$$

Now substituting equation B2 and B3 in equation 1 we have:

$$\frac{m(p_i) - m(p_{wf})}{q_g} = \frac{1637.43T}{kh}\log(t) + \frac{1637.43T}{kh}\log(\frac{0.0063k}{\phi\mu c_t A}) + \frac{575.2T}{kh} + \frac{1422TS}{kh} \text{....(B4)}$$

where the slope is:

$$\text{slope} = \frac{1637.43T}{kh} \quad \text{.....(B5)}$$

Skin calculations

To calculate the skin values shown on Fig. 4.6 and Fig. 4.12, we took the analytical pseudo-pressure equation (B1), and from the intercept (t = 1 day) of each semi-log straight line (neglecting the first two points due to simulation errors) of the plot of $m(p_i)-m(p_{wf})/q_g$ versus log time, we calculated the skin values (equation B6).

$$\text{intercept} = \frac{1637.43T}{kh}\log\left(\frac{0.0063k}{\phi\mu c_t r_w^2}\right) + \frac{575.2T}{kh} + \frac{1422TS}{kh} \quad \text{.....(B6)}$$

***OGIP* calculations**

To calculate the original gas in place (*OGIP*) in Fig. 4.17 and Fig. 4.23 we refer to Ibrahim *et al.*[28] (equation B7). To apply this equation, the slope at the end of transient period (Ibrahim e*t al.*, $\tilde{m}_{PSS}$**)** from plotting $m(p_i)-m(p_{wf})/q_g$ versus superposition time shown in Fig. 4.28. Fig. 4.28 shows the plot for $\gamma = 0$. In Fig. B1 the tangent at the end of the transient period is shown. The slope of the tangent is $\tilde{m}_{PSS}$ which is used on the equation B7 to calculate *OGIP*.

$$OGIP = \frac{2p_i S_{gi}}{Z_i(\mu_g c_t)_i}\left(\frac{1}{\tilde{m}_{PSS}}\right) \quad \text{.....(B7)}$$

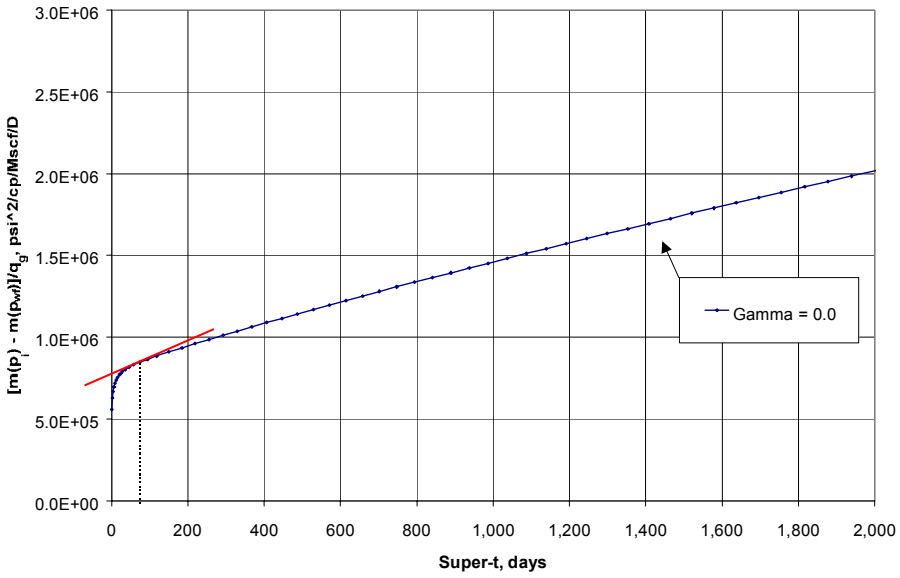

Fig. B1 Zoomed view of Fig. 4.14 $m(p_i)$-$m(p_{wf})/q_g$ as a function of Superposition time for a finite acting reservoir producing at constant p_{wf}. The tangent at the end of the transient period is shown as a solid red line.

APPENDIX C

Real Gas Diffusivity Equation Considering *k(p)*

Starting from the continuity equation to derive the diffusivity equation for a real gas:

$$\nabla \bullet \rho\vec{u} = -\frac{\partial}{\partial t}(\phi\rho) \quad \text{.....(C1)}$$

Using Darcy's law for single phase horizontal flow:

$$\vec{u} = -\frac{k}{\mu}\nabla p \quad \text{.....(C2)}$$

then substituting C2 into C1:

$$\nabla \bullet \rho\left(\frac{k}{\mu}\nabla p\right) = \frac{\partial}{\partial t}(\phi\rho) \quad \text{.....(C3)}$$

and gas density is expressed as:

$$\rho = \frac{pM}{zRT} \quad \text{.....(C4)}$$

then substituting C4 into C3:

$$\nabla \bullet \left(\frac{pM}{zRT}\right)\left(\frac{k}{\mu}\nabla p\right) = \frac{\partial}{\partial t}\left(\phi\frac{pM}{zRT}\right) \quad \text{.....(C5)}$$

Canceling the constant terms:

$$\nabla \bullet \frac{kp}{z\mu}\nabla p = \frac{\partial}{\partial t}\left(\frac{\phi p}{z}\right) \quad \text{.....(C6)}$$

The previous equation is non-linear because *p, z*, and μ depend on the solution variable, *p*. Because of that, the real gas pseudo-pressure equation, *m(p)*, is introduced as:

$$m(p) = \int_{p_o}^{p} \frac{2p'}{z(p')\mu(p')} dp' \quad \text{.....(C7)}$$

Including *k(p)*, the modified pseudo-pressure equation, $\tilde{m}(p)$, is:

$$\tilde{m}(p) = 2\int_{p_o}^{p} \frac{pk}{z\mu} dp \quad \text{.....(C8)}$$

Denoting any derivative of $\tilde{m}$ with respect to any variable, say ξ, is:

$$\frac{d\tilde{m}}{d\xi} = \frac{2pk}{z\mu}\frac{dp}{d\xi} \quad \text{.....(C9)}$$

Therefore:

$$\nabla\tilde{m} = \frac{2pk}{z\mu}\nabla p \quad \text{.....(C10)}$$

Multiplying equation C6 by 12 on both sides:

$$\nabla \bullet \frac{2kp}{z\mu}\nabla p = 2\frac{\partial}{\partial t}\left(\frac{\phi p}{z}\right) \quad \text{.....(C11)}$$

Substituting equation C10 into C11:

$$\nabla \bullet \nabla \tilde{m} = 2\frac{\partial}{\partial t}\left(\frac{\phi p}{z}\right) \text{.....(C12)}$$

$$\nabla^2 \tilde{m} = 2\left[\phi \frac{d}{dp}\left(\frac{p}{z}\right) + \frac{p}{z}\frac{d\phi}{dp}\right]\frac{\partial p}{\partial t} \text{.....(C13)}$$

Multiplying by $z\mu/2pk$ and by $2pk/z\mu$ in the right side:

$$\nabla^2 \tilde{m} = 2\frac{z\mu}{2pk}\left[\phi \frac{d}{dp}\left(\frac{p}{z}\right) + \frac{p}{z}\frac{d\phi}{dp}\right]\frac{2pk}{z\mu}\frac{\partial p}{\partial t} \text{.....(C14)}$$

$$\nabla^2 \tilde{m} = \frac{z\mu}{pk}\left[\phi \frac{d}{dp}\left(\frac{p}{z}\right) + \frac{p}{z}\frac{d\phi}{dp}\right]\frac{\partial \tilde{m}}{\partial t} \text{.....(C15)}$$

$$\nabla^2 \tilde{m} = \frac{\mu\phi}{k}\left[\frac{z}{p}\frac{d}{dp}\left(\frac{p}{z}\right) + \frac{1}{\phi}\frac{d\phi}{dp}\right]\frac{\partial \tilde{m}}{\partial t} \text{.....(C16)}$$

Knowing that:

$$c = \frac{1}{\rho}\frac{d\rho}{dp} \text{.....(C17)}$$

Substituting equation C4 into equation C17:

$$c = \frac{zRT}{pM}\frac{d}{dp}\left(\frac{pM}{zRT}\right) \text{.....(C18)}$$

$$c = \frac{z}{p}\frac{d}{dp}\left(\frac{p}{z}\right) \text{.....(C19)}$$

and:

$$c_f = \frac{1}{\phi}\frac{d\phi}{dp} \quad \text{.....(C20)}$$

substituting equations C19 and C20 into equation C16:

$$\nabla^2 \tilde{m} = \frac{\mu\phi}{k}\left[c + c_f\right]\frac{\partial \tilde{m}}{\partial t} \quad \text{.....(C21)}$$

Finally, the real gas diffusivity question considering the variation of permeability with pressure, *k(p)*, is:

$$\nabla^2 \tilde{m} = \frac{\mu\phi}{k} c_t \frac{\partial \tilde{m}}{\partial t} \quad \text{.....(C22)}$$

Where

$$c_t = c + c_f \quad \text{.....(C23)}$$

APPENDIX D

Rock Stresses Near a Wellbore

Deily and Owens[18] and Vairogs[1], as well as others have investigated the state of stress around a wellbore in a porous media.

The stress equations for this study were adapted from Lubinski. He defined macrostress, σ, as the average intensity of force per unit of total area, and microstress, σ', as the average intensity of force per unit area of the interpore material. A third type of stress represents the component of the macrostress that is primarily responsible for permeability and porosity changes; it will be called effective macrostress, σ'''.

According to Lubinski, strain in a porous medium subjected to formation stresses (macrostresses) and pore pressure is:

$$\varepsilon_r = \frac{1}{E}[\sigma_r - \nu(\sigma_\theta + \sigma_z)] + \frac{1-2\nu}{E}(1-\beta-\phi)p \quad \text{.....(D1)}$$

$$\varepsilon_\theta = \frac{1}{E}[\sigma_\theta - \nu(\sigma_r + \sigma_z)] + \frac{1-2\nu}{E}(1-\beta-\phi)p \quad \text{.....(D2)}$$

$$\varepsilon_z = \frac{1}{E}[\sigma_z - \nu(\sigma_r + \sigma_\theta)] + \frac{1-2\nu}{E}(1-\beta-\phi)p \quad \text{.....(D3)}$$

where

$$\beta = \frac{(1-2\nu_i)/E_i}{(1-2\nu)/E} \quad \text{.....(D4)}$$

The shear strain is given by:

$$\gamma_{r\theta} = \frac{1}{G}\tau_{r\theta} \quad \text{.....(D5)}$$

$$\gamma_{z\theta} = \frac{1}{G}\tau_{z\theta} \quad \text{.....(D6)}$$

$$\gamma_{rz} = \frac{1}{G}\tau_{rz} \quad \text{.....(D7)}$$

There are similarities between thermal studies and these relationships for which impermeable bodies are subjected to temperatures and surface forces. Because of this similarity, equations from thermal stress studies can be modified and used to determine stresses in porous rock.

With the thermal stress equations, the trial macrostress near a wellbore can be described as:

$$\sigma_r = (1-\beta)\frac{1-2\nu}{1-\nu}\frac{1}{r^2}\left[\frac{r^2-r_w^2}{r_d^2-r_w^2}\bullet\int_{r_w}^{r_d} prdr - \int_{r_w}^{r} prdr\right]$$
$$-\frac{r_w^2 r_d^2(p_w-p_d)}{r_d^2-r_w^2}\frac{1}{r^2} + \frac{r_w^2 p_w - r_d^2 p_d}{r_d^2-r_w^2} + \phi p \quad \text{.....(D8)}$$
$$+\frac{r_d^2}{r_d^2-r_w^2}\left(\frac{r_w^2}{r^2}-1\right)(\sigma_f - p_d)$$

$$\sigma_\theta = (1-\beta)\frac{1-2\nu}{1-\nu}\frac{1}{r^2}\left[\frac{r^2-r_w^2}{r_d^2-r_w^2}\bullet\int_{r_w}^{r_d} prdr - \int_{r_w}^{r} prdr - pr^2\right]$$
$$-\frac{r_w^2 r_d^2(p_w-p_d)}{r_d^2-r_w^2}\frac{1}{r^2} + \frac{r_w^2 p_w - r_d^2 p_d}{r_d^2-r_w^2} + \phi p \quad \text{.....(D9)}$$
$$+\frac{r_d^2}{r_d^2-r_w^2}\left(\frac{r_w^2}{r^2}+1\right)(\sigma_f - p_d)$$

$$\sigma_z = (1-\beta)\frac{1-2\nu}{1-\nu}\left(\frac{2}{r_d^2 - r_w^2}\int_{r_w}^{r_d} prdr - p\right) + \phi p - \sigma_0 \quad \text{.....(D10)}$$

Because of symmetry, the shear stresses are zero. Note that the three stress components depend on the pressure distribution, which is to be determined. Assuming that the macrostresses can be determined, lets now consider how microstresses and effective stresses are determined from them.

Macrostresses and microstresses are related as follows:

$$\sigma_r^{'} = \frac{\sigma_r}{1-\phi} \quad \text{.....(D11)}$$

$$\sigma_\theta^{'} = \frac{\sigma_\theta}{1-\phi} \quad \text{.....(D12)}$$

$$\sigma_z^{'} = \frac{\sigma_z}{1-\phi} \quad \text{.....(D13)}$$

For the moment, consider only $\sigma_r^{'}$. It can be divided into two components so that:

$$\sigma_r^{'} = p + \sigma_r^{''} \quad \text{.....(D14)}$$

But substituting for the microstress, $\sigma_r^{'}$, gives:

$$\sigma_r^{''} = \frac{\sigma_r}{1-\phi} - p \quad \text{.....(D15)}$$

The original microstress in the r direction can be looked as the sum of two microstresses having magnitudes of p and $\sigma_r^{''}$. Similarly in the other two directions:

$$\sigma_{\theta}'' = \frac{\sigma_{\theta}}{1-\phi} - p \quad \text{.....(D16)}$$

$$\sigma_{z}'' = \frac{\sigma_{z}}{1-\phi} - p \quad \text{.....(D17)}$$

It is fine to assume that porosity and rock permeability do not vary appreciably by pressure completely surrounding the rock cube. The changes in porosity and permeability, then vary mainly because of σ''_r , σ''_θ , σ''_z. The corresponding macrostresses, called effective stresses, are:

$$\sigma_{r}''' = (1-\phi)\sigma_{r}'' = \sigma_{r} - (1-\phi)p \quad \text{.....(D18)}$$

$$\sigma_{\theta}''' = (1-\phi)\sigma_{\theta}'' = \sigma_{\theta} - (1-\phi)p \quad \text{.....(D19)}$$

$$\sigma_{z}''' = (1-\phi)\sigma_{z}'' = \sigma_{z} - (1-\phi)p \quad \text{.....(D20)}$$

Effective stresses are the ones that were produced by the authors in the laboratory experiments to obtain the data discussed previously. During the laboratory tests, the effective stresses (or confining pressure) were equal in all transverse directions. Then, in relating the rock permeabilities produced in the laboratory to permeabilities in the reservoir, the following assumption was made:

$$\sigma_{c} \cong \frac{1}{2}\left(\sigma_{z}''' + \sigma_{\theta}'''\right) \quad \text{.....(D21)}$$

VITA

Name:	Mariela Franquet Barbara
Permanent Address:	California Norte, Av.Barcelona, Qta.Diana Caracas, Edo. Miranda Venezuela
Email:	marielafranquet@hotmail.com
Education:	B. S., Geophysical Engineering, Universidad Simón Bolívar, Baruta, Venezuela (November 1999) M.S., Petroleum Engineering Texas A&M University College Station, TX 77843-3116, U.S.A. (May 2004)